University of Reading

The effect of increased convective entrainment on Asian monsoon biases in the MetUM General Circulation Model

Article

Published Version

Creative Commons: Attribution 3.0 (CC-BY)

Open Access (Early Online)

Bush, S. J., Turner, A. G. ORCID: https://orcid.org/0000-0002-0642-6876, Woolnough, S. J. ORCID: https://orcid.org/0000-0003-0500-8514, Martin, G. M. and Klingaman, N. P. ORCID: https://orcid.org/0000-0002-2927-9303 (2015) The effect of increased convective entrainment on Asian monsoon biases in the MetUM General Circulation Model. Quarterly Journal of the Royal Meteorological Society, 141 (686). pp. 311-326. ISSN 1477-870X doi: https://doi.org/10.1002/qj.2371 Available at https://centaur.reading.ac.uk/36151/

It is advisable to refer to the publisher's version if you intend to cite from the work. See Guidance on citing.

To link to this article DOI: http://dx.doi.org/10.1002/qj.2371

Publisher: Royal Meteorological Society

All outputs in CentAUR are protected by Intellectual Property Rights law, including copyright law. Copyright and IPR is retained by the creators or other copyright holders. Terms and conditions for use of this material are defined in the End User Agreement.

University of Reading

www.reading.ac.uk/centaur

CentAUR

Central Archive at the University of Reading

Reading's research outputs online

RMetS
Royal Meteorological Society

The effect of increased convective entrainment on Asian monsoon biases in the MetUM general circulation model

Stephanie J. Bush,[a,b]* Andrew G. Turner,[a] Steven J. Woolnough,[a] Gill M. Martin[b] and Nicholas P. Klingaman[a]

[a]*NCAS-Climate, Department of Meteorology, University of Reading, UK*
[b]*Met Office, Exeter, UK*

*Correspondence to: S. J. Bush, Department of Meteorology, University of Reading, Earley Gate, Reading, RG6 6BB, UK. E-mail: s.j.bush@reading.ac.uk

This article is published with the permission of the Controller of HMSO and the Queen's Printer for Scotland.

We demonstrate that summer precipitation biases in the South Asian monsoon domain are sensitive to increasing the convective parametrization's entrainment and detrainment rates in the Met Office Unified Model. We explore this sensitivity to improve our understanding of the biases and inform efforts to improve convective parametrization. We perform novel targeted experiments in which we increase the entrainment and detrainment rates in regions of especially large precipitation bias. We use these experiments to determine whether the sensitivity at a given location is a consequence of the local change to convection or is a remote response to the change elsewhere. We find that a local change leads to different mean-state responses in comparable regions. When the entrainment and detrainment rates are increased globally, feedbacks between regions usually strengthen the local responses. We choose two regions of tropical ascent that show different mean-state responses, the western equatorial Indian Ocean and western north Pacific, and analyse them as case-studies to determine the mechanisms leading to the different responses. Our results indicate that several aspects of a region's mean state, including moisture content, sea surface temperature and circulation, play a role in local feedbacks which determine the response to increased entrainment and detrainment.

Key Words: Asian monsoon precipitation; convective parametrization; tropical convection; climate models

Received 4 July 2013; Revised 6 March 2014; Accepted 20 March 2014; Published online in Wiley Online Library

1. Introduction

The Asian monsoon is one of the most significant global manifestations of the seasonal cycle. In India, the summer monsoon provides nearly 80% of the total annual rainfall. Changes in the timing and intensity of the monsoon consequently have direct socio-economic impacts in South Asia.

Reliable dynamical models are essential for improving our understanding and prediction of monsoon rainfall and circulation. While most general circulation models (GCMs) capture the overall seasonal migration of tropical rain, fidelity in representing the detailed spatial, interannual and intraseasonal variation of Asian monsoon precipitation remains low (Randall *et al.*, 2007; Annamalai *et al.*, 2007; Sperber *et al.*, 2013). In this study, we address the impact of changing convective entrainment and detrainment rates on seasonal mean Asian monsoon precipitation biases in the Met Office Unified Model (MetUM, section 2).

Significant, systematic biases in seasonal mean monsoon rainfall are common in GCMs. Evaluations of GCMs including the third coupled model intercomparison project (CMIP3; Annamalai *et al.*, 2007; Bollasina and Nigam, 2009) and CMIP5 (Sperber *et al.*, 2013) as well as individual studies have shown that many monsoon precipitation biases in atmosphere-only GCMs (AGCMs) are very similar to biases in their atmosphere–ocean coupled (AOGCM) counterparts. This indicates that lack of coupling is not responsible for the rainfall biases, and studies have shown that cold biases in sea-surface temperature (SST) introduced by coupling may exacerbate them (Levine and Turner, 2012; Levine *et al.*, 2013). One particularly persistent bias is excess precipitation in the western equatorial Indian Ocean (WEIO), especially just south of the Arabian Sea (Gadgil and Sajani, 1998; Bollasina and Ming, 2012), which is related to poor representation of the competition between equatorial and continental convergence zones during the monsoon (Sperber

© 2014 The Authors and Crown copyright. *Quarterly Journal of the Royal Meteorological Society* published by John Wiley & Sons Ltd on behalf of the Royal Meteorological Society.

This is an open access article under the terms of the Creative Commons Attribution License, which permits use, distribution and reproduction in any medium, provided the original work is properly cited.

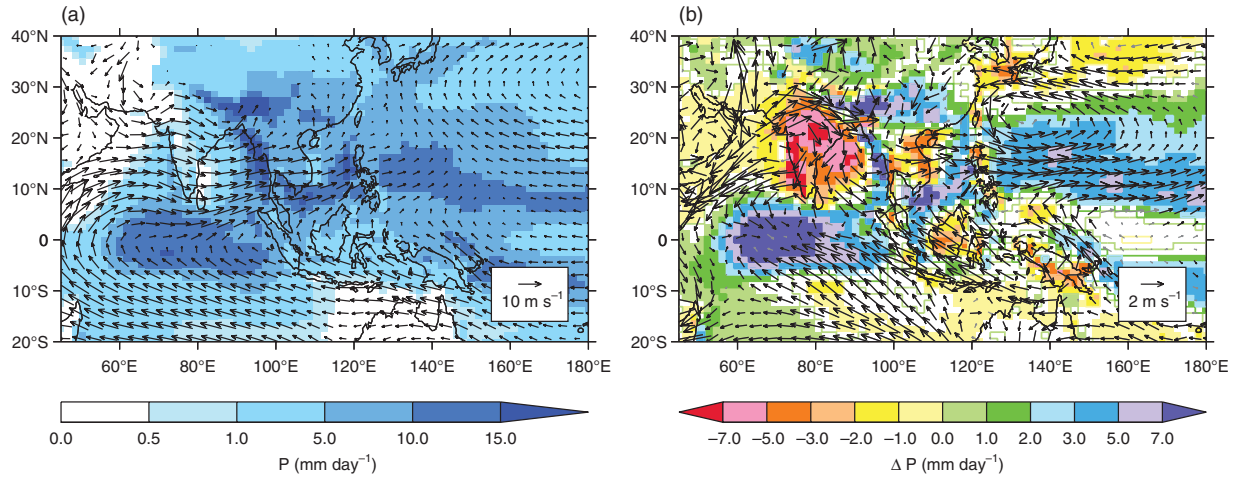

Figure 1. (a) JJAS precipitation (shading, mm day^{-1}) and 850 hPa winds (arrows, m s^{-1}) in our control integration (section 2). (b) Bias with respect to GPCP precipitation and ERA-Interim 850 hPa winds. Shaded grid points in (b) indicate precipitation biases are significant at the 95% level using a Student's *t*-test, less significant changes are outlined. Black (grey) arrows indicate either the zonal or meridional wind biases are significant (not significant) at the 95% level.

and Palmer, 1996; Gadgil and Sajani, 1998; Bollasina and Nigam, 2009). While the bias over the equatorial Indian Ocean is particularly large, there are several other important biases in the region, including low precipitation over the Indian subcontinent and excess precipitation along the southern slopes of the Himalayas and over the Western Ghats (Gadgil and Sajani, 1998). These biases are present in current versions of the MetUM, as shown in Figure 1.

Several studies have indicated that the WEIO precipitation bias is linked to other deficiencies in GCM Asian monsoon precipitation. AGCM sensitivity experiments that reduce the May WEIO diabatic heating indicate that an improvement in WEIO rainfall biases would significantly improve biases over India as well (Bollasina and Ming, 2012). Winter and spring northern Indian Ocean cold SST biases, prevalent in the CMIP3 and CMIP5 models, are connected through atmospheric circulation to the excessive convergence and precipitation biases in the WEIO (Marathayil *et al.*, 2013). These biases limit early season Indian monsoon precipitation by lowering the moisture supply over India (Levine *et al.*, 2013; Marathayil *et al.*, 2013).

In the MetUM, many systematic errors appear in short-time-scale numerical weather prediction (NWP) forecasts as well as long-time-scale climate simulations (Martin *et al.*, 2010), indicating that deficiencies in the parametrization of atmospheric subgrid-scale processes may be the underlying cause of many biases in atmospheric models. Monsoon precipitation is particularly sensitive to the subgrid-scale parametrization of convective precipitation. Authors have shown in NWP (Slingo *et al.*, 1988), seasonal (Deb *et al.*, 2007) and climate integrations (e.g. Slingo *et al.*, 1994; Rajendran *et al.*, 2002; Mukhopadhyay *et al.*, 2010) that the choice of convective parametrization schemes significantly impacts monsoon biases. Turner and Slingo (2009) suggest this sensitivity to convective parametrization is responsible for discrepancies in the simulated sensitivity of monsoon precipitation extremes to increased CO_2 in the CMIP3 models.

Even changes in individual parameters in a convection scheme can have a pronounced effect on GCM output. Parameters controlling the strength of convective entrainment contribute a large portion of model uncertainty (Sanderson and Shell, 2010; Murphy *et al.*, 2011; Klocke *et al.*, 2011). Large perturbed physics ensembles of the Hadley Centre Coupled Model, version 3 (HadCM3L) and the HadAM3 AGCM coupled to a slab ocean indicate that the uncertainty in the entrainment rate coefficient has a large influence on global-mean cloud, albedo and water vapour feedbacks (Sanderson and Shell, 2010) and the overall climate change feedback strength (Murphy *et al.*, 2011). A similar study with the ECHAM5 (ECMWF model, Hamburg version) AGCM found that uncertainty in the entrainment rate contributes a large portion of model error in simulating the present-day distribution of clouds, radiation and precipitation globally (Klocke *et al.*, 2011).

In a GCM convective parametrization, mixing entrainment and mixing detrainment rates control the amount warm, moist, ascending convective plumes mix with air aloft which is typically colder and drier. Increasing these rates increases the convection scheme's sensitivity to environmental moisture by decreasing plume buoyancy, which requires dry environments to moisten or destabilise to maintain the same precipitation rate. The immediate, one-dimensional response to increasing the entrainment and detrainment rates is typically to suppress convective precipitation until sufficient moistening, heating or dynamical forcing has occurred. How feedbacks within a GCM modify this immediate response determines the equilibrium response. Several processes could be responsible for overcoming the suppression, including moistening by shallow convection or congestus (e.g. Derbyshire *et al.*, 2004), dynamical moistening at mesoscales and larger scales (e.g. Hohenegger and Stevens, 2013; Kumar *et al.*, 2013), or convective organisation by dynamical forcing such as land–sea breezes. However, it is questionable how well GCMs represent these processes at standard resolutions with common convection schemes.

Using a set of idealised case-studies, Derbyshire *et al.* (2004) show that GCM convection schemes are less sensitive to environmental moisture than cloud-resolving models (CRMs), giving rise to excess precipitation in dry environments. Sahany *et al.* (2011) used simplified plume calculations and GCM experiments to demonstrate that a relatively high entrainment rate is required to correctly represent the dependence of the initiation of deep convection on moisture and temperature.

The sensitivity of the GCMs to the entrainment rate, and the demonstration that modelled precipitation is largely too insensitive to moisture, has motivated several studies examining the effect of increased entrainment on model bias. Increasing, changing the formulation, or placing a lower bound on the entrainment rate has a positive impact on the representation of the Madden–Julian Oscillation (MJO) in several models through suppressing precipitation in drier environments, allowing moistening to pre-condition the atmosphere for the active MJO phase (Bechtold *et al.*, 2008; Kim *et al.*, 2011; Hannah and Maloney, 2011; Del Genio *et al.*, 2012; Hirons *et al.*, 2013a,b; Klingaman and Woolnough, 2014). Neale *et al.* (2008) demonstrate in the coupled Community Climate System Model version 3 (CCSM3) GCM that adding a representation of entrainment to a previously undilute mass flux scheme and adding convective momentum transport (CMT) improves the

© 2014 The Authors and Crown copyright. *Quarterly Journal of the Royal Meteorological Society* published by John Wiley & Sons Ltd on behalf of the Royal Meteorological Society.

representation of the El Niño Southern Oscillation (ENSO), through changes to the mean state and increased MJO activity.

Increasing the entrainment rate has also been shown to have a pronounced effect on the mean state, improving some aspects and degrading others (Terray, 1998; Chikira, 2010; Kim *et al.*, 2011; Hirons *et al.*, 2013a; Oueslati and Bellon, 2013). Several authors demonstrate a beneficial decrease in precipitation along the South Pacific Convergence Zone (SPCZ) and an improvement in the double Intertropical Convergence Zone (ICTZ) precipitation bias (Terray, 1998; Chikira, 2010; Oueslati and Bellon, 2013). However, upper-tropospheric cold biases are introduced in several models (Mapes and Neale, 2011; Hirons *et al.*, 2013a).

Terray (1998) and Oueslati and Bellon (2013) note that increased entrainment increases deep convection in many convergence zones. They argue this is due to increased moisture flux into convergence zones from subsidence zones, because of an enhanced humidity–convection feedback. However, in a study of ten GCMs with a wide spread in intraseasonal variability (ISV) created by changing the threshold entrainment rate, Kim *et al.* (2011) find that increasing ISV is correlated with changes in the mean state, in particular, decreasing boreal summer precipitation over the equatorial Indian Ocean (EIO) and increasing precipitation over the Western North Pacific (WNP). This demonstrates that opposing mean-state responses are observed in some convergence zones.

Similar mean-state changes in the WEIO and WNP were observed in the MetUM by Klingaman and Woolnough (2014) during their study on the effect of increased entrainment on the MJO. In light of the importance of reducing the persistent excess precipitation bias in the WEIO for improved modelling of the Asian monsoon, we perform experiments with the MetUM to analyse the reasons for the beneficial impact in the WEIO and explore why increasing the entrainment rate has such marked, and markedly different, impacts in different regions. We use unique sensitivity experiments where we increase entrainment locally in regions of especially large bias to separate the local response of regions to increased entrainment from teleconnections and analyse the local response. We also perform initialised integrations of global and local experiments to analyse the evolution of the response as the model comes into steady state.

Section 2 describes the configuration of the MetUM used, the convective parametrization scheme in the MetUM and our experimental design. In section 3, we describe the response of the model when the entrainment rate is increased globally. In section 4, we show results of the local experiments. In section 5, we examine a series of diagnostics to understand why altering the entrainment produces different mean-state changes in two regions of interest, the WEIO and the WNP. We conclude in section 6.

2. Method

2.1. The Unified Model

We use a version of the Unified Model (MetUM), the Met Office's general circulation model. Specifically, we use the Global Atmosphere 3.0 (GA3.0) configuration of the atmospheric component of the HadGEM3 family of models. GA3.0 is a choice of atmospheric MetUM dynamical core, atmospheric parametrizations and model options (Walters *et al.*, 2011). This configuration of the MetUM is used operationally for both NWP and seasonal forecasting. Details of the model and its physical parametrizations are described in Walters *et al.* (2011). Here, we describe in detail the convective parametrization which is particularly relevant to this work.

2.2. Convective parametrization

Convective parametrization in the MetUM is derived from the bulk mass flux scheme developed by Gregory and Rowntree (1990). The scheme's foundation is single-plume parcel theory modified to represent the average properties of an ensemble of convective plumes. The scheme triggers convection from the boundary layer using an undilute parcel calculation, then performs shallow or deep convection for grid points where convection is triggered. Mid-level convection can be triggered from levels in the free troposphere.

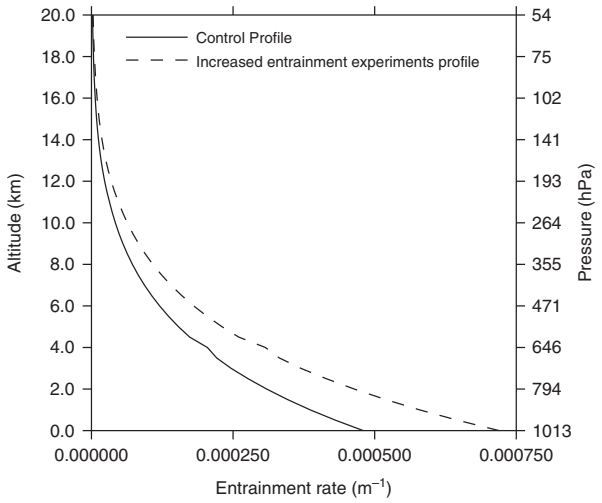

Figure 2. The fractional mixing entrainment rate profile for mid-level and deep convection in the configuration of the MetUM used in this study. The solid (dashed) line is the default (increased) profile for an ICAO standard atmosphere.

Several adjustments to the deep convection scheme have been introduced since Gregory and Rowntree (1990), such as the addition of downdraughts (Gregory and Allen, 1991), convective momentum transport using a flux gradient approach (Stratton *et al.*, 2009) and a convective available potential energy (CAPE) closure scheme, which uses a dilute CAPE calculation, based on Fritsch and Chappell (1980a,b). The time-scale for the CAPE closure is fixed at 90 minutes unless very high large-scale vertical velocities are detected in the column, when the time-scale is reduced to ensure numerical stability.

The shallow convection scheme uses a Grant (2001) closure based on a turbulent kinetic energy budget. Shallow convective momentum transport uses flux-gradient relationships derived from cloud-resolving models of shallow convection (Grant and Brown, 1999). Walters *et al.* (2011) give a full description of the MetUM convection scheme and how it couples to other aspects of the model. The configuration used here has a few additional modifications, including a requirement that undilute ascent is diagnosed for at least three vertical layers to trigger convection and slight changes to energy corrections.

Entrainment and detrainment are calculated independently by the deep, mid-level and shallow portions of the scheme. Mixing entrainment for mid-level and deep convection decreases with height according to

$$\epsilon = 4.5\, F \frac{p(z)\, \rho(z)\, g}{p_*^2}, \tag{1}$$

where ϵ is the fractional mixing entrainment rate per unit length, p and ρ are the pressure and density as a function of altitude, p_* is the surface pressure and F is an adjustable parameter that we will subsequently refer to as the 'entrainment factor'. In the default configuration, $F = 0.9$. The default entrainment rate profile is shown in Figure 2 for an ICAO standard atmosphere (WMO, 1966).

Detrainment is divided into two components. Mixing detrainment, the evaporation of moist plume air due to mixing with drier environmental air, is the natural counterpart of mixing entrainment. Forced detrainment is the representation of some convective plumes in the ensemble terminating while others

© 2014 The Authors and Crown copyright. *Quarterly Journal of the Royal Meteorological Society* published by John Wiley & Sons Ltd on behalf of the Royal Meteorological Society.

continue to ascend. As evaporation is sensitive to humidity, deep convective mixing detrainment (δ_m) is related to the entrainment by the relative humidity (RH) (Derbyshire *et al.*, 2011):

$$\delta_m = 1.5(1 - RH)\,\epsilon. \quad (2)$$

Equation (2) shows that mixing detrainment exceeds mixing entrainment when $RH < 1/3$, determining the height at which the plume mass flux decreases. Mid-level mixing detrainment instead follows the formula

$$\delta_m = \left(1 - \frac{1}{1.5F}\right)\epsilon, \quad (3)$$

where the entrainment factor, F, is the same adjustable parameter as in Eq. (1). Forced detrainment is related to the loss in buoyancy of the plume over time as described in Derbyshire *et al.* (2011).

2.3. Experimental design

The MetUM is run in atmosphere-only configuration with atmospheric resolution of 1.875° longitude by 1.25° latitude (N96), with 85 levels in the vertical and a time step of 20 min. All integrations are atmospheric model intercomparision project (AMIP) style, forced by monthly varying SSTs. In the control integration F is set to 0.9, the default value. Following a study by Klingaman and Woolnough (2014), which showed that multiplying the entrainment factor, F, by 1.5 (increasing it to 1.35) greatly improved the MetUM's tropical intraseasonal variability, we investigate the effects of $1.5F$ on the mean state of the Asian summer monsoon. The resulting mid-level and deep convective entrainment profile is increased by a factor of 1.5 and is shown under an ICAO standard atmosphere by the dashed line in Figure 2. As shown in Eqs (2) and (3), this increases the shallow and deep mixing detrainment rate profiles by a factor of 1.5, and increases the mid-level mixing detrainment profile by a factor of approximately 2.9. In our version of the MetUM, mid-level convective precipitation is common over the Indian peninsula and east Asia, but it is uncommon in the main oceanic regions we discuss in this study (not shown). There is also very little shallow convective precipitation in the MetUM over the areas we discuss.

We show results from experiments where F is increased at every model grid point and where F is increased only for selected grid points.

Integrations to study the equilibrium response in AMIP-style integrations are run from September 1978 to December 1998. The first four months are discarded to eliminate spin-up effects, leaving 20 years of data. To analyse the summer response as it evolves to steady state, we conduct a set of initialised increased entrainment factor experiments. We use 01 July outputs from the control integration for each of the 20 years to initialise 20 increased entrainment factor integrations which are run for two months. The experiments used in this study are summarised in Table 1.

2.4. Significance testing

We employ two techniques to determine the significance of changes in experiments relative to interannual variability. The first is a Student's t-test which determines the likelihood that the two sample means are drawn from the same normal distribution.

The second uses a binomial distribution, which gives the likelihood of a number of 'yes' events out of a number of trials, in trials where the only possible outcomes are yes and no. This is used to calculate the significance of the sign, rather than the magnitude, of a change in mean value. The number of positive values and the number of negative values in a sample are counted and the probabilities of each number are calculated according to a binomial distribution. If either probability is less than 10%, the sign of a change is considered significant.

Table 1. Experiments analysed in this study. AMIP-style experiments are run for 20 years, and initialised experiments are a set of two-month experiments initialised from 20 years of 01 July conditions. Section 2.3 gives details.

Experiment	Domain of entrainment factor increase	Experiment types
Global	All grid points	AMIP-style and Initialised
WEIO	50–90°E, 10°S–5°N	AMIP-style and Initialised
WNP	Ocean grid points in 123–175°E, 5–27°N	AMIP-style and Initialised
Land	All land grid points	AMIP-style only

2.5. Observational datasets

In order to evaluate our control integration, we use the Global Precipitation Climatology Project (GPCP) version 2 Monthly Precipitation Analysis (Adler *et al.*, 2003) to assess mean precipitation. It is a merged analysis which incorporates precipitation estimates from low-orbit satellite microwave data, geosynchronous-orbit satellite infrared data and surface rain-gauge observations at 2.5°× 2.5° resolution.

We use the European Centre for Medium-Range Weather Forecasts (ECMWF) ERA-Interim atmospheric reanalysis product (Dee *et al.*, 2011) to assess circulation at 850 hPa, vertical velocities and moist static energy budget terms. All observed products were bilinearly interpolated to the MetUM grid for comparison.

3. Response of the monsoon mean state to increased entrainment and detrainment

Asian monsoon rain falls primarily in June, July, August and September (JJAS). The JJAS mean tropical Indo-Pacific precipitation and 850 hPa circulation in the control integration are shown in Figure 1(a). Rainfall is most prevalent over the equatorial Indian Ocean, just off the west coast of India, in the Bay of Bengal, in the western north Pacific, over India itself and on the south slopes of the Himalayas. There are significant biases in MetUM precipitation in almost all of these regions, shown in Figure 1(b). Many of these biases are common in GCMs, in particular the excess precipitation over the equatorial Indian Ocean and the lack of precipitation over the Indian subcontinent (Annamalai *et al.*, 2007; Sperber *et al.*, 2013). The distribution of biases in the MetUM broadly agrees with the CMIP5 multi-model mean (Sperber *et al.*, 2013), though in the MetUM there is a larger precipitation excess in the equatorial Indian Ocean and it is more evenly distributed across the Equator. There is also a larger deficit in precipitation over the Indian subcontinent. Precipitation biases over the WNP are similar.

The change in JJAS tropical Indo-Pacific precipitation when the convective parametrization's entrainment factor is increased by a factor of 1.5 is shown in Figure 3. Precipitation decreases along the equatorial Indo-Pacific, extending from the WEIO across the Maritime Continent and along the SPCZ. Precipitation also decreases over subtropical Asia, particularly along the southern slopes of the Himalayas and in eastern China. In contrast, in the WNP there is a very large increase in precipitation. Precipitation increases to a lesser extent in the northern Bay of Bengal and over the west coast of the Indian peninsula. Precipitation changes are accompanied by changes in circulation. In the Indo-Pacific, the largest changes at 850 hPa are increased westerly flow from the western Indian Ocean, Indian subcontinent and Maritime Continent to the WNP and increased cyclonic circulation over eastern Asia and the WNP. Precipitation decreases slightly in much of the rest of the equatorial Tropics, including central America, the eastern equatorial Pacific, western equatorial Atlantic and equatorial Africa, while parts of the subtropics, such as the Gulf of Mexico and the southwestern Pacific, show slight increases in precipitation (not shown).

© 2014 The Authors and Crown copyright. *Quarterly Journal of the Royal Meteorological Society* published by John Wiley & Sons Ltd on behalf of the Royal Meteorological Society.

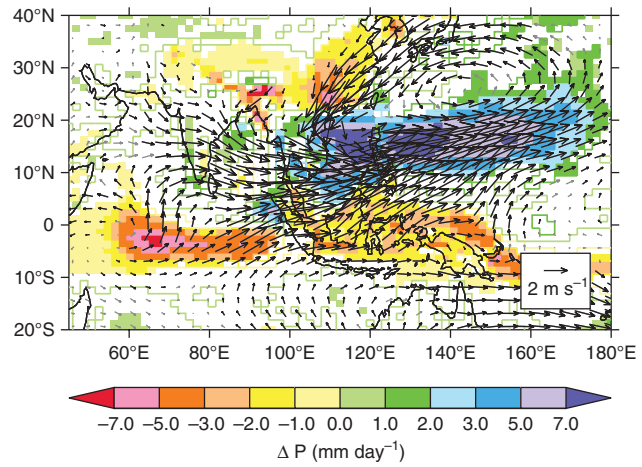

Figure 3. The response of JJAS tropical Indo-Pacific precipitation (shading, mm day^{-1}) and 850 hPa circulation (arrows, m s^{-1}) to multiplying the entrainment factor (and consequently the entrainment and detrainment rates) by 1.5 in the MetUM. Significance is indicated as in Figure 1.

The precipitation response to increased entrainment in the MetUM is similar to that in other GCMs (Terray, 1998; Chikira, 2010; Kim *et al.*, 2011; Oueslati and Bellon, 2013). While in all models precipitation increases in the western tropical Pacific, in the ARPEGE (Action de Recherche Petite Echelle Grande Echelle) AGCM this increase occurs on the Equator (Oueslati and Bellon, 2013), whereas in our model the increase occurs north of the Equator.

To quantify precipitation changes, we bilinearly interpolate the MetUM data to the GPCP grid and calculate the root-mean-square error (RMSE) and pattern correlation of precipitation in the control integration and global experiment compared to GPCP precipitation. We calculate metrics for three regions: the WEIO, the WNP and the entire domain of Figure 3 (Table 2). While increasing the entrainment factor has a number of beneficial regional impacts, over the entire domain both the amplitude and spatial pattern of precipitation degrade slightly. In the WEIO, the RMSE improves considerably, consistent with the decrease in the excess precipitation bias, while the pattern correlation degrades slightly. In the WNP both metrics worsen, consistent with the increase in the excess precipitation bias. We also calculate the RMSE and pattern correlation between ERA-Interim winds and 850 hPa combined U and V winds in the control integration and global experiment (Table 2). We bilinearly interpolate the higher-resolution ERA-Interim data to the model grid for comparison. The representation of the winds over the WEIO changes very little with the entrainment factor increase; otherwise, wind metrics show the same behaviour as the precipitation metrics. These metrics confirm that, while increasing the entrainment factor does not improve all aspects of the model, it has a positive impact over the WEIO. We are interested in determining why increasing the entrainment factor in the MetUM causes this improvement.

Figure 4 shows the zonally averaged global meridional circulation in the control integration and changes introduced when the entrainment factor is increased. The strongest tropical feature is the winter hemisphere Hadley cell with a strong ascending branch over the Tropics and northern subtropics and a dominant descending branch over the southern subtropics. Increasing the entrainment factor shifts the Hadley cell northwards, towards the summer hemisphere pole, and broadens the southern descending branch. While not discussed in detail here, an analogous result is seen in DJFM, with precipitation and ascent shifted southwards, towards the summer hemisphere pole.

The summer Hadley cell strengthening is consistent with the changes observed in increased low-level entrainment experiments with the Integrated Forecast System (Terray, 1998), but inconsistent with the mild weakening of the Hadley cell seen in experiments where the entrainment rate is increased by a factor of two in the ARPEGE model (Oueslati and Bellon, 2013).

Table 2. Root-mean-square error and pattern correlation comparing JJAS precipitation and 850 hPa wind in the control integration and global experiment to GPCP precipitation and ERA-Interim 850 hPa wind, respectively. The monsoon domain is defined as 45–180°E and 20°S–40°N, the domain of Figures 1 and 3. The WEIO domain is 50–90°E, 10°S–5°N and the WNP domain is 123–175°E, 5–27°N.

Model integration	Region evaluated	Precipitation		850 hPa wind	
		RMSE (mm day^{-1})	Pattern correlation	RMSE (m s^{-1})	Pattern correlation
Control	Monsoon	2.89	0.76	1.25	0.95
Global Experiment	Monsoon	3.57	0.69	2.06	0.89
Control	WEIO	5.36	0.69	1.03	0.98
Global Experiment	WEIO	3.69	0.61	1.02	0.98
Control	WNP	3.05	0.75	1.44	0.88
Global Experiment	WNP	6.43	0.44	3.38	0.59

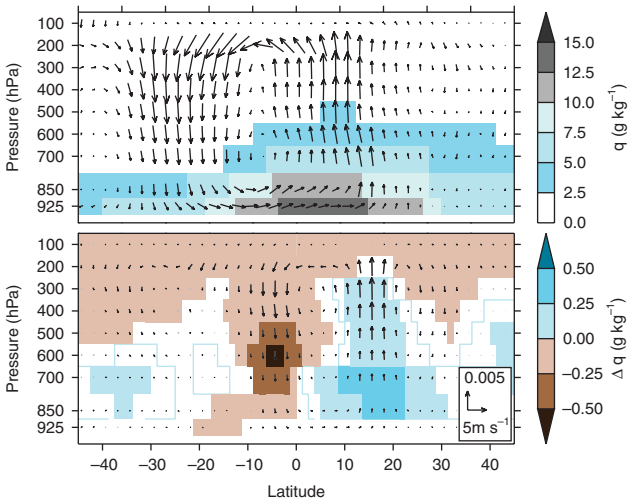

Figure 4. (a) JJAS mean specific humidity (shading, g kg^{-1}), meridional and vertical circulation (arrows, ms^{-1}) in the control integration zonally averaged over all longitudes. (b) The response to multiplying the convective entrainment factor by 1.5. Shaded precipitation changes are significant at the 95% level using a Student's t-test; less significant changes are outlined. Black (grey) arrows indicate either the U or W wind changes are significant (not significant) at the 95% level.

The longitudinal structure of these changes is shown by the 500 hPa vertical velocity (Figure 5). In the control integration, ascent occurs over most of the equatorial Indian Ocean and WNP. Increasing the entrainment factor increases ascent over the WNP, and decreases ascent over the equatorial Indian Ocean, Maritime Continent, Himalayas and east China. These changes represent an improvement in vertical velocity biases in the Indian Ocean sector, but a degradation in the WNP (not shown). Overall, increasing the entrainment factor has a neutral impact on the 500 hPa vertical velocity with respect to ERA-Interim, with the control integration having an RMSE of 0.025 Pa s^{-1} and pattern correlation of 0.76 between 50°N and 50°S, and the global experiment having an RMSE of 0.026 Pa s^{-1} and pattern correlation of 0.74 when the entrainment factor is increased.

4. Experiments locally increasing the entrainment and detrainment rates

4.1. *Motivation and description*

In a one-dimensional column of the MetUM where external forcing is held constant, we expect increased mixing entrainment and detrainment to immediately reduce convective precipitation. Increasing the entrainment and detrainment rates dilutes

© 2014 The Authors and Crown copyright. *Quarterly Journal of the Royal Meteorological Society* published by John Wiley & Sons Ltd on behalf of the Royal Meteorological Society.

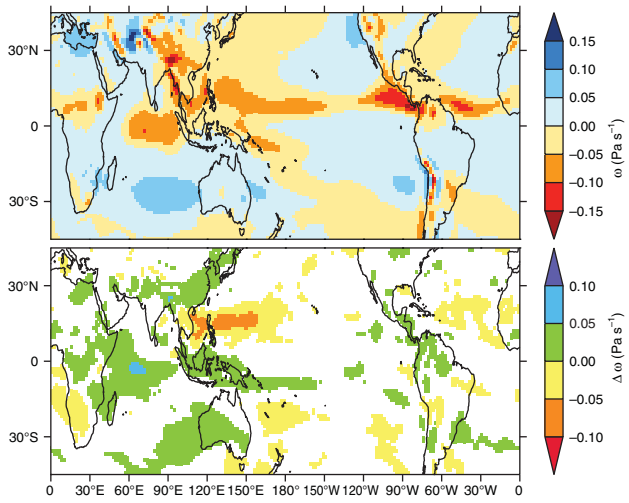

Figure 5. (a) JJAS mean of the 500 hPa vertical velocity (ω, Pa s^{-1}) in the control integration, and (b) the response to multiplying the convective entrainment factor by 1.5. Differences shown are significant at the 95% level using a Student's t-test.

moisture in an ensemble plume, reducing the moisture available in the plume for convective precipitation. The MetUM employs a CAPE closure scheme and, in almost all cases, increasing the entrainment and detrainment rates decreases an ensemble plume's dilute CAPE, causing the convection scheme to calculate lower total instability for the column. The closure consequently scales the ensemble plume's mass flux profile by reducing the cloud-base mass flux. This also reduces the cloud-base moisture flux and, accordingly, the convective precipitation. In a global model, this one-dimensional response is transient. The difficulty lies in determining how feedbacks within a region and between different regions modify the initial response to create the final, steady-state response in a region and the time-scale for this modification. The reduction in precipitation could persist to steady state or the column could increase in moisture or instability, returning the column to the control precipitation rate.

To understand the relative roles of the local response and feedbacks, we run a series of targeted experiments in which we increase the entrainment factor only in regions of interest. The simplest hypothesis in these experiments is that precipitation decreases in the targeted region and the rest of the model responds to that precipitation decrease. We target three regions individually:

- WEIO
- WNP
- all land points.

We choose the WEIO to investigate the significant decrease in the important precipitation bias there in the global experiment. We choose WNP to explore the large response there in the global experiment and to contrast with the WEIO, since the WEIO and WNP are similar regions (warm, oceanic, moist) which respond differently in the global experiment. The WEIO and WNP regions are entirely oceanic, so we also conduct an experiment where the entrainment factor is increased over all land grid points in the model, including coastal grid points. This targets the large changes in precipitation seen over the Himalayas, Maritime Continent and East Asia in the global experiment. Table 1 lists the experiments and defines the targeted regions. The JJAS mean precipitation and 850 hPa circulation changes in the AMIP-style targeted experiments are shown in Figure 6.

4.2. *Mean-state response*

Results from the AMIP-style WEIO experiment (Figure 6(a)) are consistent with the expected local effect of increasing the entrainment factor. Precipitation decreases in the WEIO which increases moisture in the Somali jet. This increases precipitation

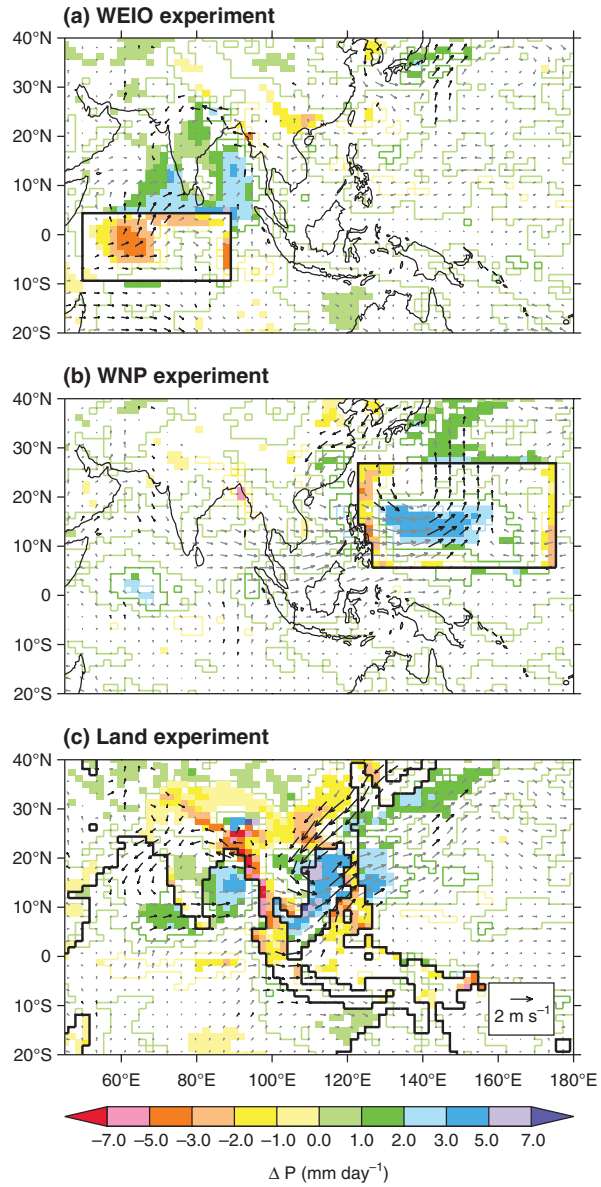

Figure 6. The response of tropical Indo-Pacific JJAS precipitation (shading, mm day^{-1}) and 850 hPa winds (arrows, m s^{-1}) in AMIP-style experiments to increasing the entrainment factor in the targeted regions: (a) the WEIO, (b) the WNP and (c) over all model land points including coasts. Increased entrainment factor regions are outlined in black. For clarity, continental outlines are omitted in (c). Significance is indicated as in Figure 1.

in the southeast Arabian Sea and Bay of Bengal where the jet exits the increased entrainment factor region. A Gill-type response to off-equatorial diabatic heating (Gill, 1980) from increasing precipitation in the Bay of Bengal strengthens the flow up the monsoon trough. This increases precipitation in central India, but the increase is only a small fraction of the MetUM bias over the Indian Peninsula. Where the mean flow (Figure 1) enters the increased entrainment factor region, precipitation decreases inside the boundary. This is consistent with our expectation that an abrupt increase in entrainment factor tends to decrease precipitation (section 4.1). Where the mean flow exits the increased entrainment factor region, we see the opposite effect, with especially large increases in precipitation within a few grid points of the boundary.

The increased precipitation in and around India is consistent with sensitivity experiments indicating that reducing erroneous diabatic heating over the Indian Ocean leads to improved monsoon circulation in GCMs (Bollasina and Ming, 2012). Analysis of observed outgoing long-wave radiation (OLR) signatures associated with intraseasonal variations indicates that the equatorial Indian Ocean and South Asian continental convection zones compete, and when one is suppressed, the other

© 2014 The Authors and Crown copyright. *Quarterly Journal of the Royal Meteorological Society* published by John Wiley & Sons Ltd on behalf of the Royal Meteorological Society.

tends to become more active (e.g. Krishnan *et al.*, 2000). This is also illustrated in our experiment as the air dried by precipitation around India returns to the Equator aloft, descending over the WEIO (not shown). The precipitation anomalies and cyclonic wind anomalies in and around India in this experiment are also consistent with interannual anomalies and intraseasonal empirical orthogonal functions (EOFs) calculated from NCEP/NCAR* reanalysis data (Sperber *et al.*, 2000), indicating that an improved representation of these modes of variability could lead to a similar pattern of improvement in the mean state.

In the AMIP-style WNP experiment (Figure 6(b)), precipitation increases near the centre of the region, but considerably less than in the global experiment (Figure 3). This suggests that increasing precipitation in the WNP in the global experiment is not purely a response to precipitation decreases elsewhere in the model, but rather a semi-local effect. As in the WEIO experiment, precipitation decreases where the mean flow enters the edges of the increased entrainment factor region (Figure 1(a)) and precipitation increases where the mean flow exits. While many of the circulation changes present in the global experiment are also present here, their magnitude is reduced, consistent with the precipitation response. Increased ascent and heating in the WNP drives anomalous westerlies from the tip of the India peninsula across the Bay of Bengal and Indochina peninsula to the WNP, as well as cyclonic circulation through the increased entrainment factor region and over East Asia. Very little change in precipitation is seen outside the increased entrainment factor region, but the meridional overturning circulation is slightly strengthened in the west Pacific (not shown).

In the AMIP-style land experiment (Figure 6(c)), precipitation primarily decreases over land, consistent with the immediate, one-dimensional effect of the entrainment change. Decreases are particularly large on the south slopes of the Himalayas, in east China, and on the northern islands of the Maritime Continent. As in previous experiments, precipitation decreases just inside the boundary of the increased entrainment factor region, and precipitation increases just outside the boundary. Since the boundaries are longer in this experiment, these 'edge effects' are more prevalent. They are especially noticeable on the west coast of the Indochina Peninsula and over the Philippines, where the low-level westerly flow crosses Southeast Asia. It would be prudent to assume responses over narrow strips of land in this experiment are primarily due to edge effects. However, changes far from the edges, such as the changes over the Himalayas, are unlikely to be edge effects given their similarity to the response in the global experiment and that, in all local experiments, edge effects appear to be confined to the few grid points nearest the edge.

The reduced convection over land in this experiment shifts precipitation just offshore to the Bay of Bengal, South China Sea, east of the Philippines, east of Japan, and west of the Indian peninsula. Ascent increases in the South China Sea while ascent decreases over east Asia and descent increases over the east Pacific (not shown). The dynamical response to increased diabatic heating over the Bay of Bengal is a strengthened monsoon trough which slightly increases precipitation over India.

The sign of the precipitation response in the global experiment (Figure 3) appears to be a simple combination of the responses in the the local experiments (Figure 6). Increasing the entrainment factor over land generally suppresses land precipitation. Increasing the entrainment factor in the WEIO decreases precipitation and increases southwesterlies out of the region, while increasing the entrainment factor in the WNP increases precipitation and increases westerlies into the WNP.

In the AMIP-style global experiment, these local responses feed back on each other to strengthen the westerlies across the India and Indochina peninsulas and strengthen the cyclonic circulation over the WNP. This carries the increased moisture in the Somali jet across the India and Indochina peninsulas, further increasing the moisture available for precipitation in the WNP. The increased ascent in the WNP and decreased ascent in the WEIO collectively strengthen the Hadley Cell and shift it northwards, which, combined with the local response over land, promotes decreased precipitation over the Maritime Continent and the SPCZ.

The increase in precipitation in the WNP does not appear to be a result of the large precipitation decreases over the WEIO or Asian continent. Instead, the local response to the increased entrainment factor in the WNP forces the WNP's surroundings, altering their state, and the altered surroundings in turn force the WNP. These 'near-local feedbacks' determine the response of the region.

4.3. *Initial local response*

We have shown that the WNP's response to an increased entrainment factor is of opposite sign to that in the WEIO, even in targeted experiments. To explore the detailed evolution of the feedbacks that are driving the mean-state response, we conduct a set of 20 2-month long initialised experiments (section 2.3). In these experiments we impose the entrainment factor increase on 01 July, after the monsoon circulation is already established, and analyse how the initial response evolves into the mean-state response. We focus on the WEIO and WNP as case-studies, to determine the mechanism generating different mean-state responses in two similar regions of tropical ascent. In Figure 7 we show the day 1 mean response in the WEIO and WNP initialised experiments. Initially, as expected from

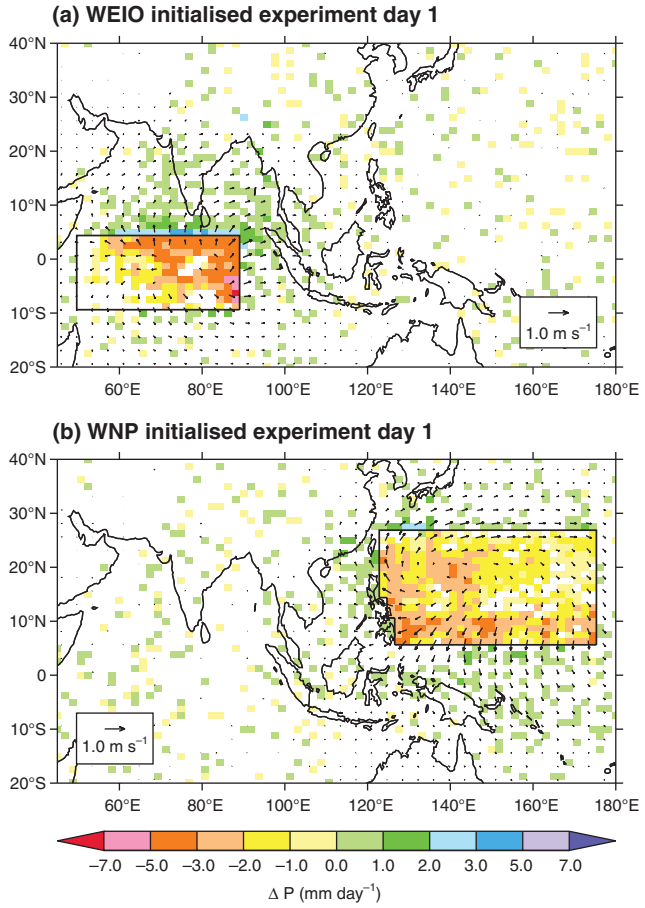

Figure 7. Twenty-year mean response of precipitation (shading, mm day^{-1}) and 850 hPa winds (arrows, m s^{-1}) on the first day the entrainment factor is increased in the (a) WEIO and (b) the WNP initialised experiments. Only changes whose sign are significant at the 10% level using a binomial distribution are shown.

*(US) National Centers for Environmental Prediction/National Center for Atmospheric Research

© 2014 The Authors and Crown copyright. *Quarterly Journal of the Royal Meteorological Society* published by John Wiley & Sons Ltd on behalf of the Royal Meteorological Society.

the immediate, one-dimensional effect of increased entrainment factor, precipitation decreases in both regions. The different locations of the regions leads to different initial dynamical responses to decreased latent heating. The WEIO demonstrates an approximate Gill-type response to equatorial decreased latent heating, which results in a pair of anticyclones to the north and south and increased easterlies and westerlies out of the increased entrainment factor region. The mean flow (Figure 1(a)) carries the excess moisture which results from decreased precipitation to the northeast, out of the experimental region, where it increases rainfall. The WNP demonstrates a Gill-type response to decreased off-equatorial latent heating, which results in an anticyclone centred on the region. Small precipitation increases surround the region.

In Figure 8, we show a histogram of day 1 time-step precipitation rates in the WEIO and WNP in their local initialised experiments. We construct the histogram using every time step and grid point available. As anticipated in section 4.1, increasing the entrainment factor leads to a decrease in the preferred rates of precipitation as well as an increase in the overall frequency of precipitation events (defined as time steps with precipitation over 0.005 mm day^{-1}). We discuss the time-step precipitation rates in more detail in section 5.2.

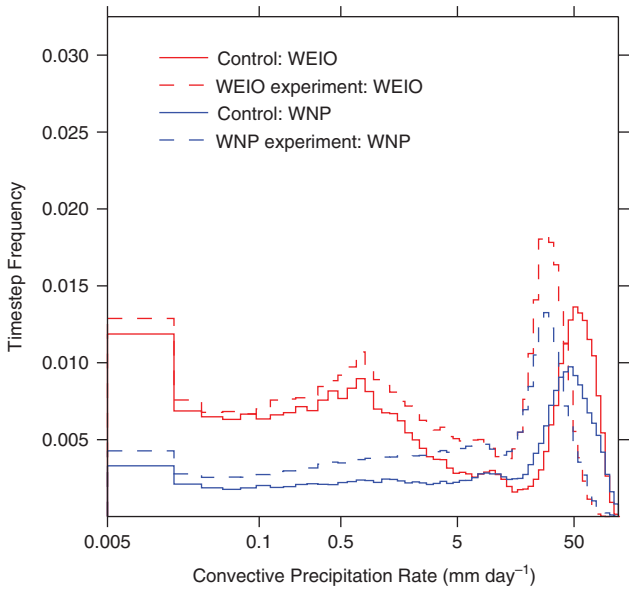

Figure 8. Histograms of time-step convective precipitation rates in the control integration (solid lines) and initialised experiments (dashed lines) on the first day that entrainment factor is increased in the WEIO (red) and WNP (blue). Every grid point in the WEIO and WNP regions at every time step on 01 July in a 20-year set of experiments is included. The numbers of events less than 0.005 mm day^{-1} are not shown; their frequencies are 65% in the control in the WEIO, 58% in the experiment in the WEIO, 79% in the control in the WNP, and 74% in the experiment in the WNP. This figure is available in colour online at wileyonlinelibrary.com/journal/qj

The initial precipitation response in the WEIO is broadly consistent with the JJAS mean response in Figures 3 and 6(a), but the initial precipitation and dynamical responses in the WNP are the opposite of those in the JJAS mean. While the regions initially respond similarly, this shows they evolve differently. The daily evolution of the precipitation and dynamical responses in the WNP initialised experiment are shown in Figure 9. The initial precipitation decrease and resulting anticyclone persist until approximately day 5, after which the precipitation increase and cyclonic response seen in the global and WNP AMIP-style experiments (Figures 3 and 6(b)) slowly develop. This evolution is purely driven by the increase in entrainment and detrainment in the WNP.

5. Diagnostics of response in the WEIO and WNP to the global entrainment factor increase

Section 4.2 demonstrates that, in the WEIO and WNP, the AMIP-style response to increasing the entrainment factor locally (Figure 6) is consistent with the AMIP-style response to increasing the entrainment factor globally (Figure 3). Section 4.3 further shows that the WNP and the WEIO initially respond similarly to increased entrainment factor and that while the initial response broadly persists to the mean state in the WEIO, in the WNP the initial response reverses about 5 days after the entrainment factor is increased. This motivates a more thorough study of the behaviour in and around the two regions in the global experiments. Here we analyse a series of diagnostics including moisture budgets, changes in time-step precipitation rates, and the relationship between precipitation and moisture to determine how the increased entrainment and detrainment rates, the initial states of the regions and feedbacks lead to the different steady-state responses.

5.1. *Evolution of moisture and MSE budgets*

Figure 10 shows the evolution of daily mean precipitation and 850 hPa circulation in the Indo-Pacific region in a 20-year set of initialised experiments where the entrainment factor is increased

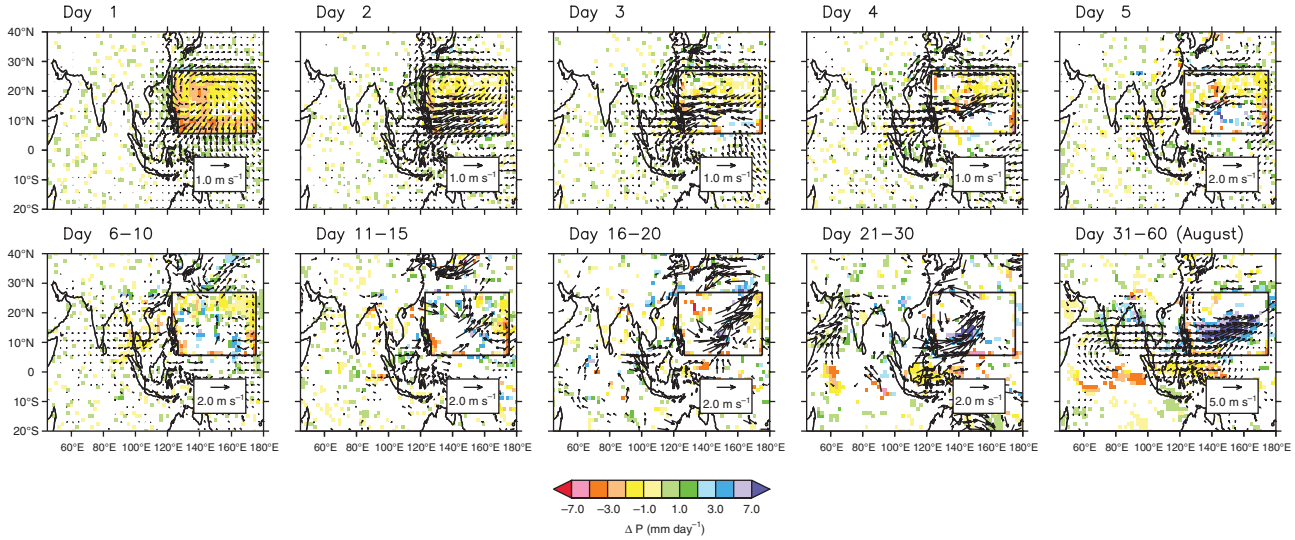

Figure 9. Twenty-year mean evolution of changes in precipitation (shading, mm day^{-1}) and 850 hPa circulation (arrows, m s^{-1}) in the WNP initialised experiment. Only changes whose sign are significant at the 90% level are shown. The reference wind speed increases from 1 to 5 m s^{-1} through the panels.

© 2014 The Authors and Crown copyright. *Quarterly Journal of the Royal Meteorological Society* published by John Wiley & Sons Ltd on behalf of the Royal Meteorological Society.

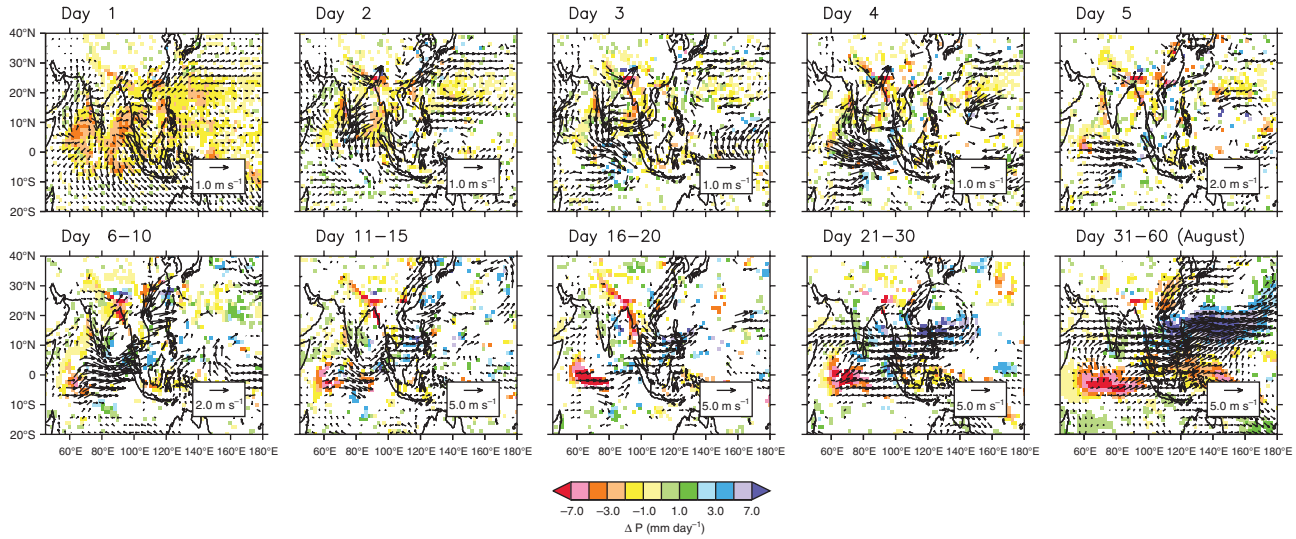

Figure 10. As Figure 9, but for the global initialised experiment. The reference wind speed increases from 1 to 5 m s^{-1} through the panels and is not always the same as the reference wind speed in Figure 9.

globally on 01 July. The evolution is consistent with the evolution of the local experiments, with initial drying everywhere evolving into the JJAS AMIP-style response (Figure 3) over the course of a month. To quantify this response, in Figure 11 we calculate daily mean moisture budgets averaged over the WEIO and WNP regions used in section 4. Precipitation, evaporation, horizontal moisture flux convergence (i.e. the sum of moisture convergence and advection) and approximate column water vapour (CWV, integrated from 1013 to 100 hPa with approximately 100 hPa resolution) are shown for July and August. In the control integration, August precipitation is nearly equal in the WEIO and the WNP, and moisture is supplied by a combination of evaporation and moisture convergence. In the WEIO, evaporation dominates, but in the WNP, evaporation and moisture flux are equally important. The WNP is moister than the WEIO, with a daily mean CWV approximately 20% higher.

On the first day that the entrainment factor is increased, precipitation decreases in both regions, decreasing latent heating. Decreased latent heating decreases the horizontal moisture flux convergence and increased detrainment causes an increase in CWV. Over days 2 to 4, precipitation and moisture flux rebound in response to the increased CWV and destabilisation, exceeding the values in the control integration and returning to the control values by day 5. On day 5, the CWV in the WEIO decreases to its control value, whereas the CWV in the WNP remains increased. Evaporation is also increased slightly in the WNP. Subsequently, the evolution of the WEIO and WNP differ considerably. Precipitation, horizontal moisture flux and CWV persistently decrease in the WEIO, while all three increase in the WNP. After approximately 1 month the integrations reach a steady state. At steady state, there is almost no moisture flux convergence in the WEIO and local evaporation supplies the moisture for the remaining precipitation. In the WNP, an increase in the moisture flux convergence and a small increase in evaporation supply the moisture for the large increase in precipitation. The CWV difference between the two regions grows. At steady state, daily mean CWV in the WNP is approximately 40% higher than in the WEIO.

As the moist static energy (MSE) budget is a useful diagnostic of the interaction between forcing and large-scale circulation (Neelin and Held, 1987), we show other terms in the MSE budget in Figure 11. We do not show the sensible heat flux due to its small contribution to the overall budget. In the control integration, sensible heat flux is roughly constant in time at approximately 0.4 mm day^{-1} in the WEIO and 0.25 mm day^{-1} in the WNP. When the entrainment factor is increased, sensible heat flux increases to 0.3 mm day^{-1} in the WNP. In both regions, the changes in radiation, evaporation, dry static energy (DSE) convergence and moisture flux convergence roughly balance one another as required by MSE conservation. In the WEIO (WNP) the reduction (increase) in precipitation is associated with increased (reduced) radiative cooling, which is counter-intuitive in a radiative convective equilibrium framework. This suggests that these regions are not in radiative convective equilibrium. We can understand the changes in the WEIO as a response to reduced cloudiness associated with the reduced precipitation and reduced CWV. The increased radiative cooling and reduced precipitation must be balanced by decreased dry static energy divergence associated with weaker ascent. The weaker ascent also leads to a reduced moisture convergence which balances the reduction in precipitation. The dry static energy divergence reduces more than the moisture convergence decreases, leading to a slight decrease in MSE divergence to balance the slight reduction in the diabatic MSE source. In the WNP there is a small decrease in radiative cooling and an increase in evaporation which are balanced by increased MSE divergence produced by a larger increase in DSE divergence than increase in moisture convergence.

In Table 3 we compare the August daily mean values of moisture and MSE budget terms in the control integration and global experiment to estimates from ERA-Interim reanalysis. While many of these quantities are not directly constrained by observations in the reanalysis products, they are indirectly affected through dependence on fields that are. Consistent with our comparison to GPCP in section 3, precipitation in the WEIO is in better agreement with reanalysis in the global experiment, while precipitation in the WNP is in better agreement with reanalysis in the control integration, despite the fact that GPCP precipitation exceeds ERA-Interim precipitation by approximately 2 mm day^{-1} in the WNP. The WNP MSE budget and CWV agree very well with ERA-Interim in the control integration, and very poorly in the global experiment. In contrast, the WEIO MSE budget agrees better with ERA-Interim reanalysis in the global experiment than in the control integration. However, in ERA-Interim, the moisture for WEIO precipitation is supplied by more moisture convergence and less evaporation than in the global experiment. This indicates that, while the precipitation agrees very well, there are still biases in the underlying mechanism. The WEIO is moister in ERA-Interim than in the global experiment and instead agrees well with the control integration.

In Figure 12, we use the model's tendencies to calculate the evolution of the ratio of horizontal moisture flux convergence to horizontal DSE convergence in the WEIO and WNP in the control integration and global initialised experiments. The ratios are different in the control integration; the WEIO has

© 2014 The Authors and Crown copyright. *Quarterly Journal of the Royal Meteorological Society* published by John Wiley & Sons Ltd on behalf of the Royal Meteorological Society.

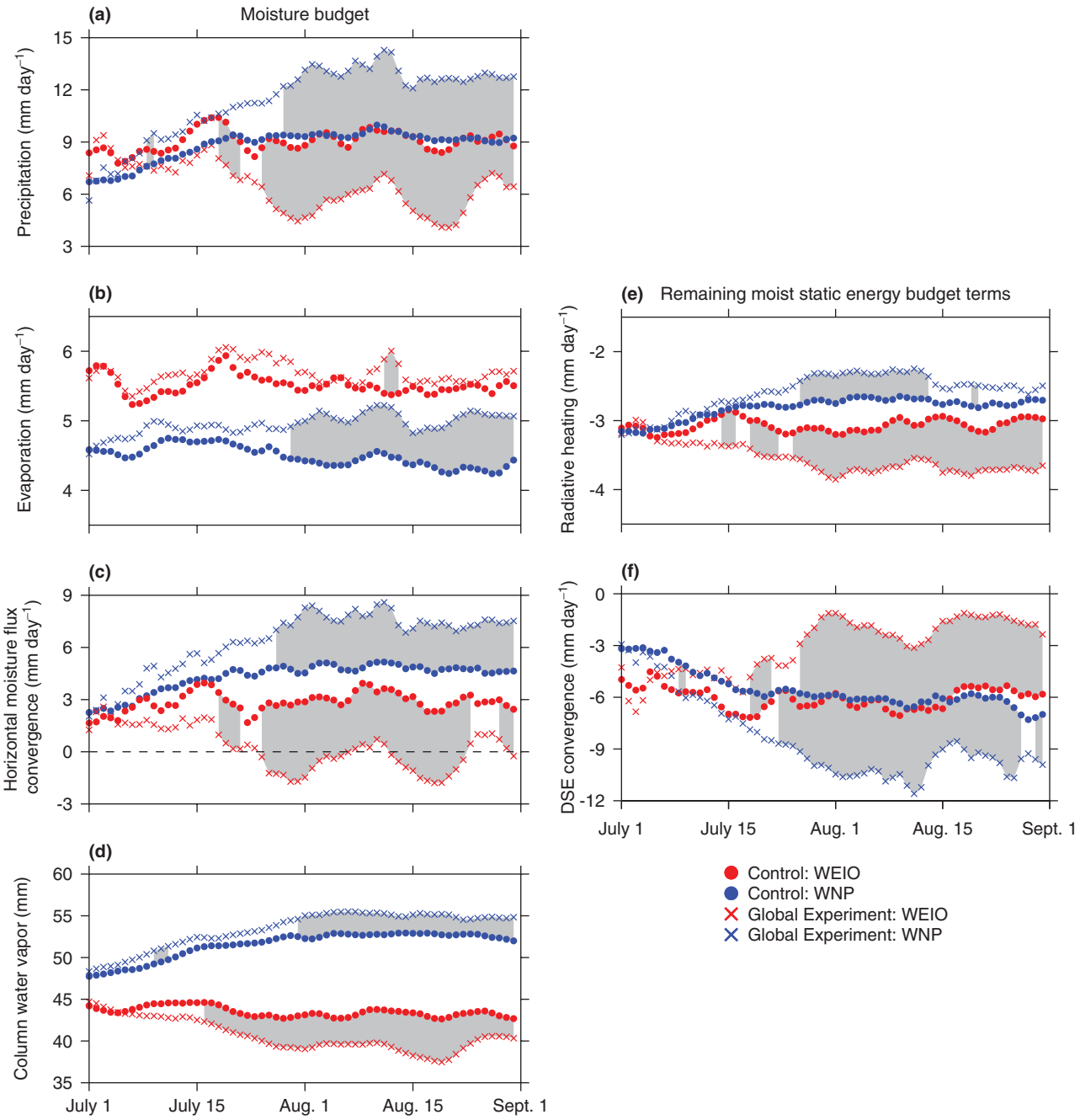

Figure 11. Twenty-year mean July and August evolution of daily (a) precipitation (mm day^{-1}), (b) evaporation (mm day^{-1}), (c) horizontal moisture flux convergence (mm day^{-1}), (d) approximate CWV (mm), (e) radiative cooling (mm day^{-1}) and (f) dry static energy (DSE) convergence (mm day^{-1}) in the control integration (dots) and global initialised experiment (crosses) averaged over the WEIO (red) and WNP (blue). Shaded changes are significant daily at the 95% level using a Student's *t*-test. In all fields, fluxes are converted to mm day^{-1} using the latent heat of evaporation ($L = 2.5 \times 10^3$ J kg^{-1}) and the size of the region. This figure is available in colour online at wileyonlinelibrary.com/journal/qj

less moisture convergence for its DSE convergence than the WNP, suggesting that there is less moisture convergence per unit mass convergence into the WEIO than in the WNP. When the entrainment factor is increased, the ratios stay the same in the WNP, while in the WEIO the ratio increases, showing even less horizontal moisture flux convergence for a given amount of DSE convergence. Sometimes, the WEIO ratio is even positive, indicating moisture flux divergence as shown in Figure 11. These differences may indicate that, due to the changed circulation and forcing after the entrainment factor is increased, drier air is being advected into the WEIO, whereas the WNP is able to continue advecting moist air, despite increased mass convergence.

This difference may be due to differences in the vertical structure of heating in the two regions, which are associated with differences in the vertical structure of moisture flux convergence. In Figure 13, we show the daily vertical velocity (ω) profiles for the WEIO and WNP in the control integration and global initialised experiments. Consistent with the precipitation changes in Figure 11, on the first day the entrainment factor is increased, vertical velocities reduce. They rebound quickly and by day 2 are, if anything, slightly increased relative to the control integration. From day 6, the ascent in the WEIO reduces and the ascent in the WNP increases. Throughout the evolution in the control integration, the shape of the WEIO profile indicates more upper-level convergence than the WNP. While in the global experiments the magnitude of the profile changes, the shape changes very little. It is likely that the greater convergence in the moist lower troposphere in the WNP profile contributes to increased moisture convergence into the WNP, allowing the region to recover from the initial decrease in precipitation more quickly, further destabilising the region and promoting convection. This is consistent with the differences in DSE convergence and moisture convergence shown in Figure 12. In Figure 14 we compare the JJAS vertical velocity profiles in the AMIP-style control integration and

© 2014 The Authors and Crown copyright. *Quarterly Journal of the Royal Meteorological Society* published by John Wiley & Sons Ltd on behalf of the Royal Meteorological Society.

Table 3. August daily mean and standard deviation of MSE budget terms in the control integration, global initialised experiment and ERA-Interim reanalysis. All units are mm day^{-1} except for CWV, which has units of mm.

	Control		Global Experiment		ERA-Interim	
	Mean	σ	Mean	σ	Mean	σ
WEIO						
CWV	43.2	3.7	39.3	3.8	45.0	2.8
Precipitation	9.17	3.25	5.70	3.11	5.73	1.56
Evaporation	5.47	0.52	5.63	0.62	4.70	0.64
Moisture convergence	3.02	3.33	−0.33	3.14	0.77	1.98
Radiation	−3.05	0.62	−3.70	0.56	−3.16	0.45
DSE convergence	−6.10	3.79	−1.85	3.43	−3.86	7.89
WNP						
CWV	52.7	2.7	55.1	2.4	52.5	2.3
Precipitation	9.33	2.82	12.98	3.46	8.71	1.85
Evaporation	4.37	0.61	5.05	0.66	4.31	0.52
Moisture convergence	4.81	2.38	7.63	2.99	4.18	1.99
Radiation	−2.72	0.47	−2.42	0.40	−2.55	0.36
DSE convergence	−6.27	3.21	−10.0	3.45	−4.88	3.78

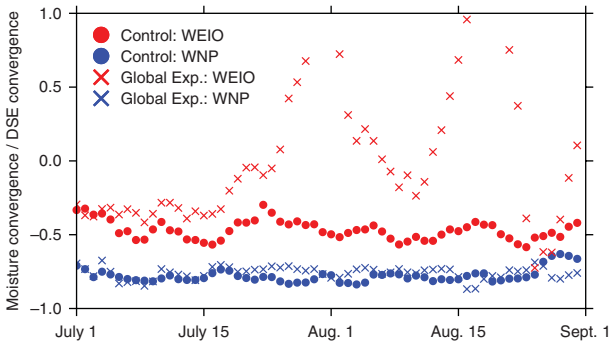

Figure 12. The ratio of horizontal moisture flux convergence to DSE convergence in the WEIO (red) and WNP (blue) for the control integration (dots) and global initialised experiments (crosses). This figure is available in colour online at wileyonlinelibrary.com/journal/qj

global experiment to ERA-Interim. In the WEIO, the magnitude and shape of the profile are in better agreement with the reanalysis in the global experiment than in the control integration. In contrast, in the WNP the magnitude and shape of the profile in ERA-Interim are in much better agreement in the control integration than in the global experiment. However, the ERA-Interim profile appears to peak slightly lower in the troposphere than in the control integration.

As shown in section 4.3 and anticipated in section 4.1, the initial decrease in precipitation due to the increased entrainment factor is associated with a decrease in the time-step intensity of convective precipitation. Reduced rainfall in a given time step results in a more unstable environment profile remaining at the end of the time step, increasing the likelihood that deep convection will be triggered in the next time step and increasing the number of time steps in which rainfall occurs. The decrease in time-step precipitation intensity therefore indicates a more uniform distribution of rainfall with time. Consequently, instead of precipitation alternating between high-intensity events and no triggered convection, the increased entrainment factor enables the model to rain more consistently at moderate rates.

We now examine whether this reduction in time-step rainfall intensity continues once the integrations reach steady state. Histograms of the time-step rain rates of convective precipitation in the WEIO and WNP after the global initialised experiments have reached a steady state are shown in Figure 15. As in the histograms of the day 1 response (Figure 8), preferred time-step precipitation rates decrease in both regions. However, the frequency of all rain events (time steps with greater than 0.005 mm day^{-1}) changes considerably over the course of the integrations in response to feedbacks. When entrainment and detrainment are increased in the WEIO, the frequency of time-step rain events increases only slightly, while in the WNP the frequency of rainfall events increases from 23% of time steps in the control integration to 45% in the global initialised experiment.

The decrease in time-step rainfall intensity does not necessarily indicate a decrease in daily rainfall amounts. If time-step rainfall intensities decrease, daily mean rainfall also decreases unless the number of time-step rainfall events increases enough to compensate. The JJAS average increase in daily mean precipitation in the WNP occurs despite lower time-step precipitation intensity, due to rainfall on more time steps in a day.

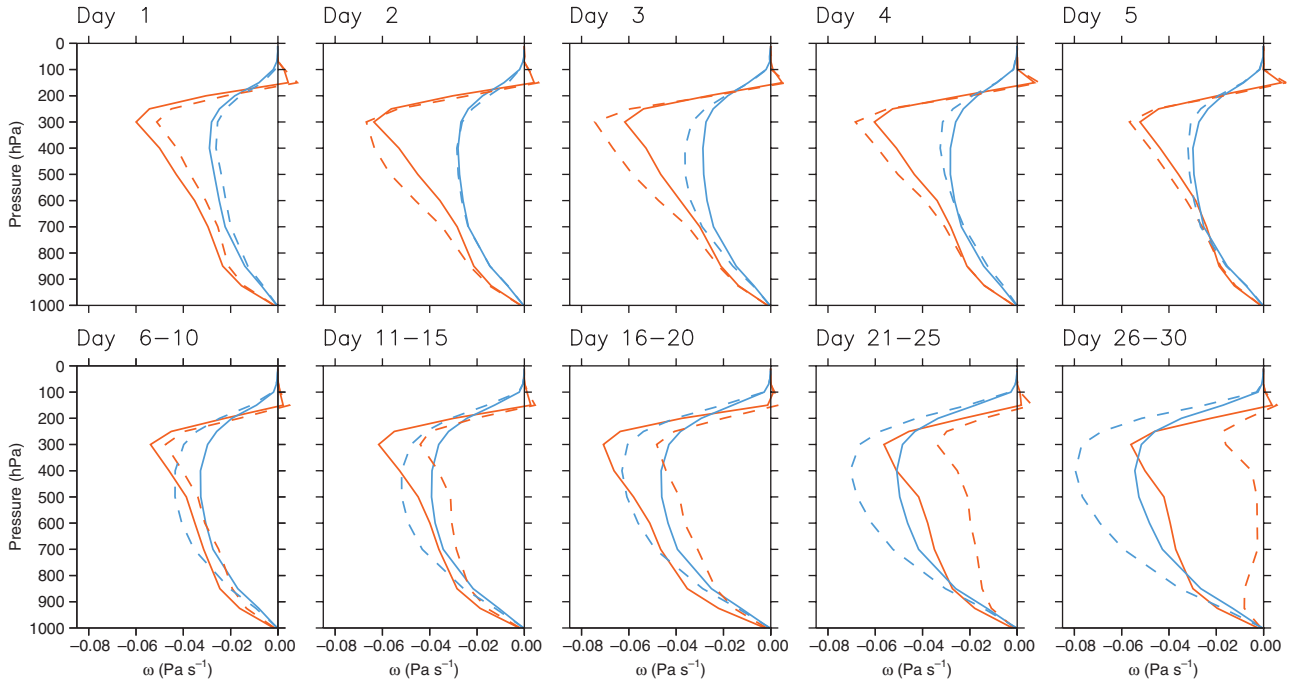

Figure 13. Evolution of 20-year mean profiles of ω (Pa s^{-1}) in the control (solid lines) and global initialised experiment (dashed lines) averaged over the WEIO (red) and WNP (blue). This figure is available in colour online at wileyonlinelibrary.com/journal/qj

© 2014 The Authors and Crown copyright. *Quarterly Journal of the Royal Meteorological Society* published by John Wiley & Sons Ltd on behalf of the Royal Meteorological Society.

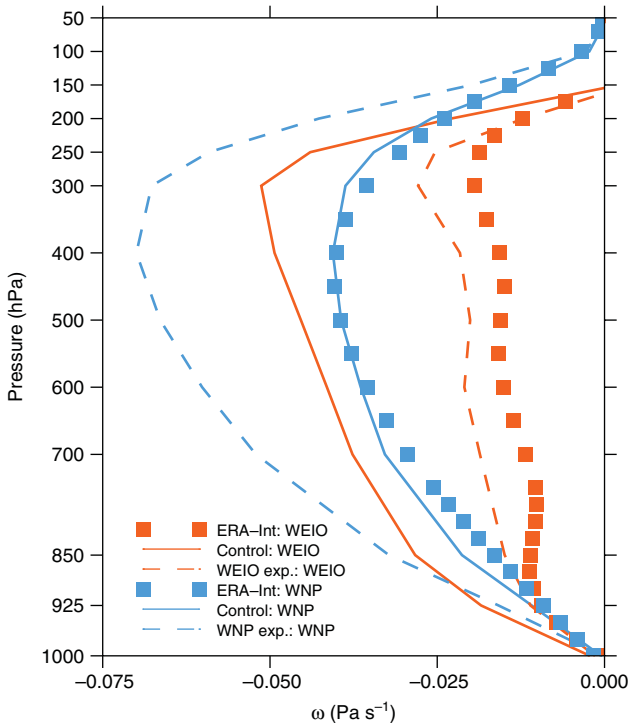

Figure 14. JJAS vertical velocity (ω, Pa s^{-1}) profile in the control integration (solid lines), global initialised experiment (dashed lines) and ERA-Interim reanalysis (squares) averaged over the WEIO (red) and WNP (blue). This figure is available in colour online at wileyonlinelibrary.com/journal/qj

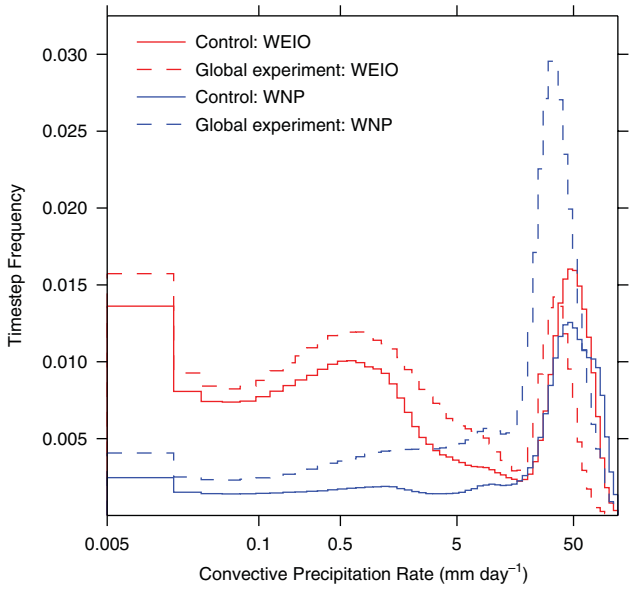

Figure 15. Histogram of time-step convective precipitation rates in the control integration (solid lines) and global initialised experiment (dashed lines). All August time steps of the 20 initialised experiments in the WEIO (red) and WNP (blue) regions are included. The numbers of events less than 0.005 mm day^{-1} are not shown; their frequencies are 58% in the control in the WEIO, 56% in the experiment in the WEIO, 77% in the control in the WNP, and 55% in the experiment in the WNP. This figure is available in colour online at wileyonlinelibrary.com/journal/qj

5.2. *Time-step precipitation rates*

5.3. *CWV and precipitation*

Increasing the entrainment and detrainment rates alters the sensitivity of convective precipitation to moisture, as the increased mixing of environment and 'plume-ensemble' air reduces the buoyancy of a plume less if the environment is also warm and moist. To characterise this change in our model, in Figure 16 we

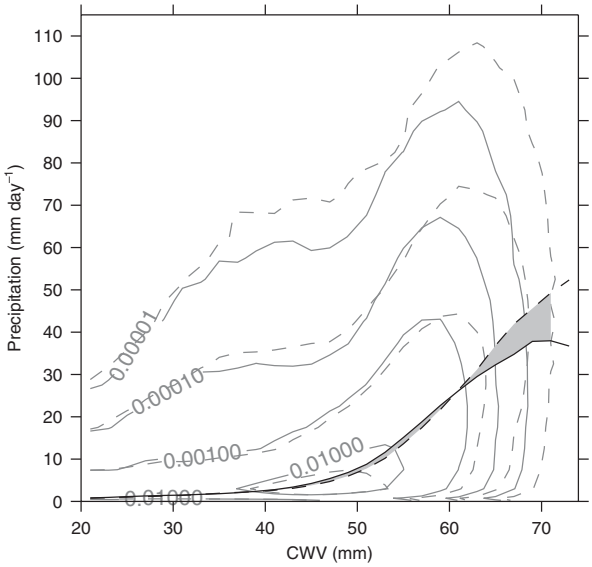

Figure 16. Grey solid (dashed) lines contour a histogram of daily CWV and precipitation in the control integration (global AMIP-style experiment) in tropical regions of ascent ($\omega < 0$ between 30°S and 30°N) over JJAS. The black solid (dashed) line is the average value of precipitation in a CWV bin in the control integration (global AMIP-style experiment). The area between the lines is shaded where the difference is significant at the 95% level using a Student's t-test.

show a histogram of the daily values of CWV and precipitation in regions of tropical ascent ($\omega < 0$ between 30°S and 30°N) for every day in the 20 JJAS seasons in the AMIP-style control integration (grey solid) and global experiments (grey dashed). There are many differences between the two distributions. The contours consistently extend to higher CWV in the global AMIP-style experiment than in the control integration, indicating precipitation over a wider range of daily CWV. At higher CWV the distribution extends to increased daily precipitation. The black solid (dashed) line is the average daily precipitation at a given CWV in the control integration (global experiment). Daily mean precipitation increases rapidly with CWV in the control integration and global experiment. Increasing the entrainment factor decreases daily mean precipitation at lower daily CWV and increases daily mean precipitation at higher daily CWV.

Figure 17 shows a histogram of the daily CWV for each grid point in the WEIO and WNP in the control integration and

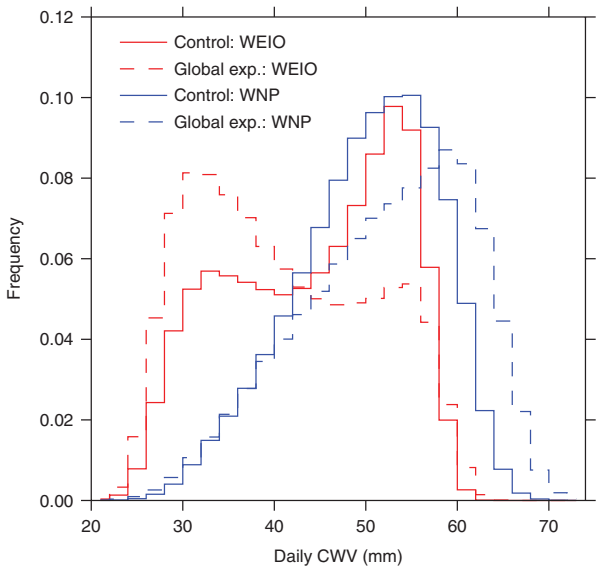

Figure 17. Histograms of daily grid point CWV (mm) for every day in every JJAS season in the control integration (solid line) and global AMIP-style experiment (dashed line). All grid points within the WEIO (red) and WNP (blue) are included. This figure is available in colour online at wileyonlinelibrary.com/journal/qj

© 2014 The Authors and Crown copyright. *Quarterly Journal of the Royal Meteorological Society* published by John Wiley & Sons Ltd on behalf of the Royal Meteorological Society.

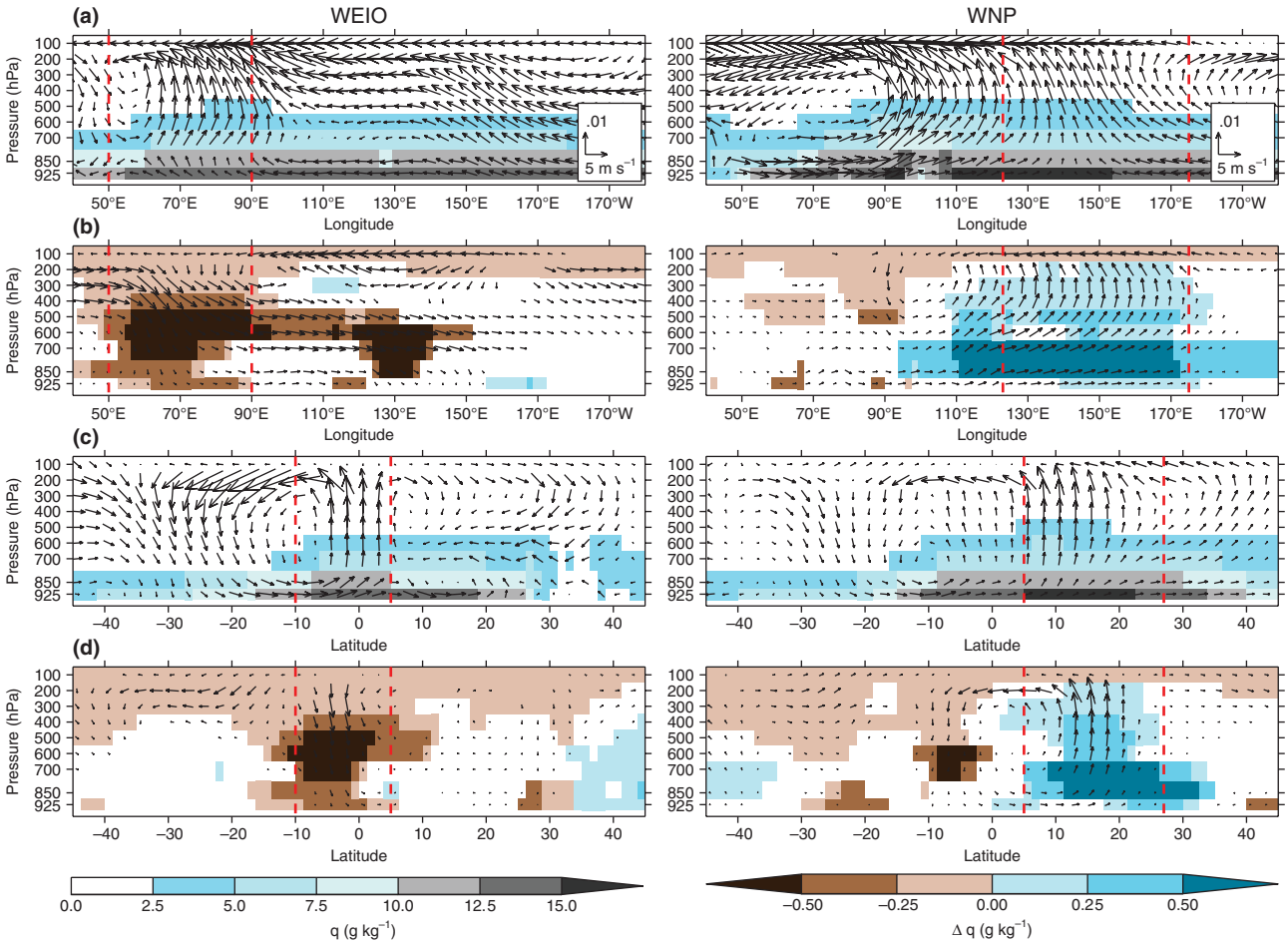

Figure 18. (a) JJAS specific humidity (shading, $g\,kg^{-1}$) and zonal circulation (arrows, $m\,s^{-1}$) meridionally averaged across the WEIO and WNP in the control integration. (b) Changes in the global AMIP-style experiment. Only changes significant at a 95% level with a Student's t-test are shown. (c, d) are as (a, b) but for meridional circulation zonally averaged. Although these are for the global experiment, the red dashed lines denote the boundaries of the WEIO and WNP regions for reference.

global AMIP-style experiments. In the WNP, the distribution of CWV in the control extends to higher CWV than in the WEIO. While the spread in the relationship between daily CWV and daily precipitation in the Tropics is large (Figure 16), the increase in precipitation at high CWV indicates that this moister initial state may be important in determining the WNP's response to increased entrainment factor. It is well established that on seasonal and interannual time-scales convection in the WNP is related to the behaviour of the North Pacific subtropical high (NPSH), such that enhanced convection in the WNP corresponds to a cyclonic anomaly and increased moisture flux into the region as the NPSH contracts to the east (Lu, 2001; Lu and Dong, 2001). A few very moist grid points that increase in precipitation may be key to initiating the precipitation–moisture flux feedback that reverses the initial anticyclonic response to the WNP entrainment factor change.

Figure 16 also illustrates that, at constant CWV, the precipitation change due to increased entrainment factor is small, until the CWV exceeds approximately 60 mm. For values of CWV below $\sim$ 60 mm, increasing CWV by even a few millimetres increases the daily mean precipitation more than increasing the entrainment factor. Figures 11 and 17 show that, in response to the entrainment factor increase, local feedbacks increase the moisture in the WNP and at steady state, a higher fraction of the region is very moist ($>$ 60 mm). This increase in moisture is clearly related to the final increase in precipitation in the region.

5.4. *Surrounding environment*

So far, we have examined the evolution and characteristics of the WEIO and WNP, and we now analyse the characteristics of their surroundings. The surrounding environment determines the characteristics of the air advected into the region when the circulation adjusts to the increased entrainment factor. The WEIO and WNP are located in very different environments. Figure 18 shows JJAS latitude and longitude sections of specific humidity and circulation averaged across the WEIO and the WNP. In the control integration, the WEIO is a narrow region of ascent in the equatorial Indian Ocean. Air is advected into the region from the moist Maritime Continent to the east (Figure 18(a)), but air advected in from the south is from a drier subtropical subsidence region (Figure 18(c)). In contrast, the WNP is a region of ascent surrounded by other regions of ascent. Warm moist air is advected into the region from the west across India and the Indochina peninsula and from the east across the West Pacific (Figure 18(a)). Additional moist air is supplied from the Maritime Continent to the south (Figure 18(c)). This suggests that there is more moisture available around the WNP to supply an increase in moisture flux and rainfall as suggested in section 5.1.

As the horizontal moisture gradient in tropical oceanic regions is influenced by the SST, Figure 19 compares the JJAS mean SSTs and horizontal circulation to the JJAS precipitation response in the global experiment. Qualitatively, where the mean flow is directed from regions of lower SST to regions of higher SST, precipitation decreases, while in regions where the mean flow is directed across regions of high SST, precipitation increases. Bollasina and Nigam (2009) and Bollasina and Ming (2012) suggest that the Indian Ocean excess precipitation bias is due to GCM precipitation being overly sensitive to Indian Ocean SST and SST gradients. While increasing the entrainment factor does not directly impact this relationship, it appears to indirectly shift the rainfall to the highest SSTs, perhaps increasing the sensitivity

© 2014 The Authors and Crown copyright. *Quarterly Journal of the Royal Meteorological Society* published by John Wiley & Sons Ltd on behalf of the Royal Meteorological Society.

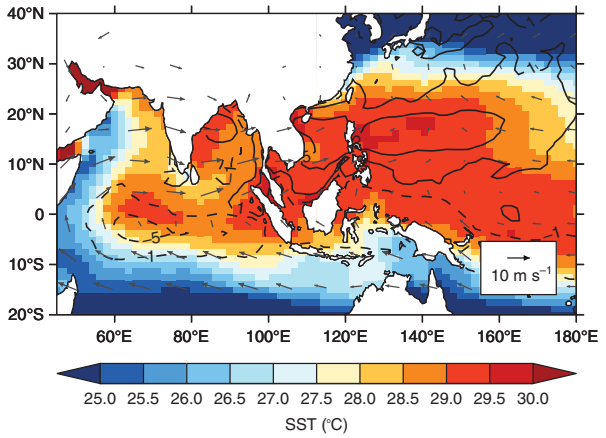

Figure 19. JJAS SSTs (shading, °C) and 850 hPa circulation (arrows, m s^{-1}) in the control integration, compared to the JJAS precipitation change over the ocean in the global AMIP-style experiment (black contours). The solid (dashed) contours are positive (negative) changes, and contours are drawn at −5, −1, 1, and 5 mm day^{-1}.

of precipitation to SSTs, but also decreasing the precipitation and consequent convergence in regions of strong SST gradients.

6. Discussion and conclusions

Increasing the fractional entrainment and detrainment rates in the MetUM's convective parametrization, as well as other GCMs (Kim *et al.*, 2011), reduces several persistent Asian summer monsoon biases while exacerbating others. While increasing entrainment and detrainment is consequently not a path to an improved representation of the monsoon, understanding the reasons for the beneficial impact on some biases may be useful for future parametrization development. We analysed experiments where we increased the entrainment and detrainment rates globally, and in targeted regions, and used them to separate the immediate, local effect of the entrainment factor change from changes in forcing.

We found that the sign of the response to a local entrainment factor increase in the WEIO, WNP and land experiments was almost always the same as the sign of the response to the global entrainment factor increase in the same locations. This indicates that individual changes are not solely determined by teleconnections, but rather are determined by the local impact of increasing the entrainment and detrainment rates and resulting near-local feedbacks. The response to globally increased entrainment and detrainment rates in the Indo-Pacific appears to be a superposition of these local responses strengthened by feedbacks.

We further analysed the WEIO and WNP as case-studies of tropical convergence regions that show different mean-state precipitation responses to increased entrainment and detrainment. The decrease in precipitation in the WEIO can be explained as persistence of the immediate, one-dimensional effect of the increased entrainment and detrainment rates, whereas the precipitation increase in the WNP is more complicated. Diagnostics indicate that precipitation increases in the moistest regions in the model. The WNP is moister initially than the WEIO, as well as moistening through feedbacks when the entrainment factor is increased. Since the MetUM convection scheme decreases time-step convective rainfall intensity when the entrainment factor is increased (section 5.2), increases in daily mean precipitation indicate rainfall over more of the day.

We also showed differences in moisture flux convergence into the two regions. The WEIO is bordered to the south by a drier, subsiding environment, while the WNP is surrounded by warm, moist ascending air. Vertical velocity profiles indicate less lower-tropospheric convergence in the WEIO, indicating that the air advected into the WEIO is likely drier than that advected into the WNP.

Luo and Stephens (2006) show that, when superparametrization is added to a GCM (SP-CAM), precipitation in the WNP is dramatically overestimated. They suggest this is due to an overactive convection–wind–evaporation feedback and demonstrate that, if evaporation is decoupled from the other variables in the model, the precipitation in the WNP decreases by 50%. It is difficult to determine from Luo and Stephens (2006) whether the important effect is in the WNP region itself, or in the surrounding regions. Since evaporation increases only slightly in the WNP when the entrainment factor is increased in our experiments, a local overactive convection–wind–evaporation feedback in the WNP can not be the explanation for the large increase in precipitation in our experiments.

The lack of ocean–atmosphere coupling in our integrations exaggerates the precipitation response in the WNP, as SSTs do not reduce in response to the increased cloud accompanying the increased precipitation. However, it is unlikely that this is responsible for the entire increase in precipitation. For example, Stan *et al.* (2010) show that when SP-CAM is coupled, the large WNP precipitation response to the superparametrization reduces, but does not disappear. A reduction in precipitation due to coupling is also likely to come at the price of a negative SST bias, as seen in the the WEIO in coupled models (Levine and Turner, 2012).

Increasing entrainment has been shown to increase intraseasonal variability in several models, including the MetUM (Kim *et al.*, 2011; Klingaman and Woolnough, 2014). Kim *et al.* (2011) suggest there is a relationship between increased intraseasonal variability and the mean-state precipitation changes in the equatorial Indian Ocean and western Pacific. The intraseasonal variabilities in these two regions have different characteristics. The WEIO is influenced by the MJO and the boreal summer intraseasonal oscillation, while the WNP has a complex relationship with the north Pacific subtropical high and frequent synoptic-scale systems. Exploration of the interplay between each of these modes of variability and the mean state may be important for understanding the behaviour in our experiments.

Initial results from aqua-planet experiments indicate that increasing the entrainment rate focuses precipitation maxima onto the SST maxima (Oueslati and Bellon, 2013, N. Klingaman, 2013; personal communication). Our experiments are consistent with this result. Bollasina and Ming (2012) suggest that the Indian Ocean wet bias is due to precipitation in GCMs being overly sensitive to SST gradients. Increasing entrainment and detrainment rates appears to be one method of decreasing the precipitation and consequent convergence in regions of strong SST gradients. Further analysis of aqua-planet experiments may allow a more detailed exploration of the mechanism driving precipitation increases in response to increased entrainment and detrainment, without the complicated feedbacks present in a full GCM.

Independent of the reason for the mean-state change, our results demonstrate that improving the precipitation bias over the WEIO has a large effect on the precipitation in and around India. If the sources of this bias could be corrected, it may improve the persistent dry bias over India present in many CMIP3/5 models (Sperber *et al.*, 2013). However, this is not the only improvement in precipitation over India in our experiments. Increasing the entrainment factor over land grid points in the model increases precipitation over the Indian peninsula through increased diabatic heating in the Bay of Bengal. This demonstrates that, counterintuitively, suppressing convection over land can lead to increased precipitation over the Indian peninsula.

Acknowledgements

SJB was supported by the Joint Weather and Climate Research Programme, a partnership between the Natural Environment Research Council (NERC) and the Met Office, under contract R8/H9/37. AGT held a NERC Fellowship,

© 2014 The Authors and Crown copyright. *Quarterly Journal of the Royal Meteorological Society* published by John Wiley & Sons Ltd on behalf of the Royal Meteorological Society.

number NE/H015655/1. SJW and NPK were supported by the National Centre for Atmospheric Science climate directorate, a collaborative centre of NERC. GM was supported by the NERC Changing Water Cycle project SAPRISE (NE/I022469/1) and the Joint DECC/Defra Met Office Hadley Centre Climate Programme (GA01101). Computing resources for running the MetUM were provided by HECToR. SJB would also like to thank Rachel Stratton for technical advice on conducting the sensitivity experiments in this article. The authors appreciate many useful comments from an anonymous referee and Christian Jakob which substantially improved the article.

The data used in this publication is available on request from the lead author.

References

Adler RF, Huffman GJ, Chang A, Ferraro R, Xie PP, Janowiak J, Rudolf B, Schneider U, Curtis S, Bolvin D, Gruber A, Susskind J, Arkin P, Nelkin E. 2003. The version-2 global precipitation climatology project (GPCP) monthly precipitation analysis (1979 –present). *J. Clim.* **4**: 1147–1167.

Annamalai H, Hamilton K, Sperber KR. 2007. The South Asian summer monsoon and its relationship with ENSO in the IPCC AR4 simulations. *J. Clim.* **20**: 1071–1092, doi: 10.1175/JCLI4035.1.

Bechtold P, Kohler M, Jung T, Doblas-Reyes F, Leutbecher M, Rodwell MJ, Vitart F, Balsamo G. 2008. Advances in simulating atmospheric variability with the ECMWF model: From synoptic to decadal time-scales. *Q. J. R. Meteorol. Soc.* **134**: 1337–1351.

Bollasina M, Ming Y. 2012. The general circulation model precipitation bias over the southwestern equatorial Indian Ocean and its implications for simulating the South Asian monsoon. *Clim. Dyn.* **40**: 3–4, doi: 10.1007/s00382-012-1347-7.

Bollasina M, Nigam S. 2009. Indian Ocean SST, evaporation, and precipitation during the South Asian summer monsoon in IPCC-AR4 coupled simulations. *Clim. Dyn.* **33**: 1017–1032, doi: 10.1007/s00382-008-0477-4.

Chikira M. 2010. A cumulus parameterization with state-dependent entrainment rate. Part II: Impact on climatology in a general circulation model. *J. Atmos. Sci.* **67**: 2194–2211, doi: 10.1175/2010JAS3317.1.

Deb SK, Upadhyaya HC, Sharma OP, Grandpeix JY. 2007. Simulation of Indian Summer Monsoon: Sensitivity to cumulus parameterization in a GCM. *Int. J. Climatol.* **27**: 1003–1045.

Dee DP, Uppala SM, Simmons AJ, Berrisford P, Poli P, Kobayashi S, Andrae U, Balmaseda MA, Balsamo G, Bauer P, Bechtold P, Beljaars ACM, Berg LVD, Bidlot J, Bormann N, Delsol C, Dragani R, Fuentes M, Geer AJ. 2011. The ERA-Interim reanalysis: Configuration and performance of the data assimilation system. *Q. J. R. Meteorol. Soc.* **137**: 553–597, doi: 10.1002/qj.828.

Del Genio AD, Chen Y, Kim D, Yao MS. 2012. The MJO transition from shallow to deep convection in CloudSat/CALIPSO data and GISS GCM simulations. *J. Clim.* **25**: 3755–3770, doi: 10.1175/JCLI-D-11-00384.1.

Derbyshire SH, Beau I, Bechtold P, Grandpiex J-Y, Piriou J-M, Redelsberger J, Soares PMM. 2004. Sensitivity of moist convection to environmental humidity. *Q. J. R. Meteorol. Soc.* **130**: 3055–3079, doi: 10.1256/qj.03.130.

Derbyshire SH, Maidens AV, Milton SF, Stratton RA, Willett MR. 2011. Adaptive detrainment in a convective parametrization. *Q. J. R. Meteorol. Soc.* **137**: 1856–1871, doi: 10.1002/qj.875.

Fritsch JM, Chappell CF. 1980a. Numerical prediction of convectively driven mesoscale pressure systems part I: Convective parameterization. *J. Atmos. Sci.* **37**: 1722–1733.

Fritsch JM, Chappell CF. 1980b. Numerical prediction of convectively driven mesoscale pressure systems part II: Mesoscale model. *J. Atmos. Sci.* **37**: 1735–1762.

Gadgil S, Sajani S. 1998. Monsoon precipitation in the AMIP runs. *Clim. Dyn.* **14**: 659–689.

Gill AE. 1980. Some simple solutions for heat-induced tropical circulation. *Q. J. R. Meteorol. Soc.* **106**: 447–462.

Grant ALM. 2001. Cloud-base fluxes in the cumulus-capped boundary layer. *Q. J. R. Meteorol. Soc.* **127**: 407–421.

Grant ALM, Brown AR. 1999. A similarity hypothesis for shallow-cumulus transports. *Q. J. R. Meteorol. Soc.* **125**: 1913–1936.

Gregory D, Allen S. 1991. The effect of convective downdrafts upon NWP and climate simulations. In *Ninth Conference on Numerical Weather Prediction*, Denver, Colorado. 122–123. American Meteorological Society: Boston, MA.

Gregory D, Rowntree PR. 1990. A mass flux convection scheme with representation of cloud ensemble characteristics and stability dependant closure. *Mon. Weather Rev.* **118**: 1483–1506.

Hannah W, Maloney E. 2011. The role of moisture –Convection feedbacks in simulating the Madden–Julian Oscillation. *J. Clim.* **24**: 2754–2770, doi: 10.1175/2011JCLI3803.1.

Hirons LC, Inness P, Vitart F, Bechtold P. 2013a. Understanding advances in the simulation of intraseasonal variability in the ECMWF model. Part II: The application of process-based diagnostics. *Q. J. R. Meteorol. Soc.* **139**: 1427–1444.

Hirons LC, Inness P, Vitart F, Bechtold P. 2013b. Understanding advances in the simulation of intraseasonal variability in the ECMWF model. Part I: The representation of the MJO. *Q. J. R. Meteorol. Soc.* **139**: 1417–1426.

Hohenegger C, Stevens B. 2013. Preconditioning deep convection with cumulus congestus. *J. Atmos. Sci.* **70**: 448–464, doi: 10.1175/JAS-D-12-089.1.

Kim D, Sobel AH, Maloney ED, Frierson DMW, Kang IS. 2011. A systematic relationship between intraseasonal variability and mean state bias in AGCM simulations. *J. Clim.* **24**: 5506–5520, doi: 10.1175/2011JCLI4177.1.

Klingaman NP, Woolnough SJ. 2014. Using a case-study approach to improve the Madden–Julian oscillation in the Hadley Centre model. *Q. J. R. Meteorol. Soc.*, doi: 10.1002/qj.2314.

Klocke D, Pincus R, Quaas J. 2011. On constraining estimates of climate sensitivity with present-day observations through model weighting. *J. Clim.* **24**: 6092–6099, doi: 10.1175/2011JCLI4193.1.

Krishnan R, Zhang C, Sugi M. 2000. Dynamics of breaks in the Indian summer monsoon. *J. Atmos. Sci.* **57**: 1354–1372.

Kumar VV, Jakob C, Protat A, May PT, Davies L. 2013. The four cumulus cloud modes and their progression during rainfall events: A C-band polarimetric radar perspective. *J. Geophys. Res.* **118**: 8375–8389, doi: 10.1002/jgrd.50640.

Levine RC, Turner AG. 2012. Dependence of Indian monsoon rainfall on moisture fluxes across the Arabian Sea and the impact of coupled model sea surface temperature biases. *Clim. Dyn.* **38**: 2167–2190, doi: 10.1007/s00382-011-1096-z.

Levine RC, Turner AG, Marathayil D, Martin GM. 2013. The role of northern Arabian Sea surface temperature biases in CMIP5 model simulations and future projections of Indian summer monsoon rainfall. *Clim. Dyn.* **41**: 155–172, doi: 10.1007/s00382-012-1656-x.

Lu R. 2001. Interannual variability of the summertime North Pacific subtropical high and its relation to atmospheric convection over the warm pool. *J. Meteorol. Soc. Jpn.* **79**: 771–783.

Lu R, Dong B. 2001. Westward extension of the North Pacific subtropical high in summer. *J. Meteorol. Soc. Jpn.* **79**: 1229–1241.

Luo Z, Stephens GL. 2006. An enhanced convection–wind–evaporation feedback in a superparameterization GCM (SP-GCM) depiction of the Asian summer monsoon. *Geophys. Res. Lett.* **33**: 1–4, doi: 10.1029/2005GL025060.

Mapes B, Neale R. 2011. Parameterizing convective organization to escape the entrainment dilemma. *J. Adv. Model. Earth Syst.* **3**: 1–20, doi: 10.1029/2011MS000042.

Marathayil D, Turner AG, Shaffrey LC, Levine RC. 2013. Systematic winter SST biases in the northern Arabian Sea in HiGEM and the CMIP3 models. *Environ. Res. Lett.* **8**: 014028, doi: 10.1088/1748-9326/8/1/014028.

Martin GM, Milton SF, Senior CA, Brooks ME, Ineson S. 2010. Analysis and reduction of systematic errors through a seamless approach to modeling weather and climate. *J. Clim.* **23**: 5933–5957, doi: 10.1175/2010JCLI3541.1.

Mukhopadhyay P, Taraphdar S, Goswami B, Krishnakumar K. 2010. Indian summer monsoon precipitation climatology in a high-resolution regional climate model: Impacts of convective parameterization on systematic biases. *Weather and Forecasting* **25**: 369–387, doi: 10.1175/2009WAF2222320.1.

Murphy JM, Sexton DMH, Barnett DN, Jones GS, Webb MJ, Collins M, Stainforth DA. 2011. Quantification of modelling uncertainties in a large ensemble of climate change simulations. *Nature* **430**: 768–772, doi: 10.1038/nature02770.1.

Neale RB, Richter JH, Jochum M. 2008. The impact of convection on ENSO: From a delayed oscillator to a series of events. *J. Clim.* **21**: 5904–5924, doi: 10.1175/2008JCLI2244.1.

Neelin JD, Held I. 1987. Modeling tropical convergence based on the moist static energy budget. *Mon. Weather Rev.* **115**: 3–12.

Oueslati B, Bellon G. 2013. Convective entrainment and large-scale organization of tropical precipitation: Sensitivity of the CNRM-CM5 hierarchy of models. *J. Clim.* **26**: 2931–2946, doi: 10.1175/JCLI-D-12-00314.1.

Rajendran K, Nanjundiah RS, Srinivasan J. 2002. Comparison of seasonal and intraseasonal variation of tropical climate in NCAR CCM2 GCM with two different cumulus schemes. *Meteorol. Atmos. Phys.* **79**: 57–86.

Randall D, Wood R, Bony S, Colman R, Fichefet T, Fyfe J, Kattsov V, Pitman A, Shukla J, Srinivasan J, Stouffer R, Sumi A, Taylor K. 2007. Climate models and their evaluation. In *Climate Change 2007: IPCC Working Group I: The Physical Science Basis*, Chapter 8, Solomon S, Qin D, Manning M, Chen Z, Marquis M, Averyt KB, Tignor M, Miller HL. (eds.). Cambridge University Press: Cambridge, UK and New York, NY, 590–662.

Sahany S, Neelin JD, Hales K. 2011. Temperature–moisture dependence of the deep convective transition as a constraint on entrainment in climate models. *J. Atmos. Sci.* **69**: 1340–1358, doi: 10.1175/JAS-D-11-0164.1.

Sanderson BM, Shell KM. 2010. Climate feedbacks determined using radiative kernels in a multi-thousand member ensemble of AOGCMs. *Clim. Dyn.* **35**: 1219–1236, doi: 10.1007/s00382-009-0661-1.

Slingo JM, Mohanty UC, Tiedtke M, Pearce RP. 1988. Prediction of the 1979 summer monsoon onset with modified parameterization schemes. *Mon. Weather Rev.* **116**: 328–346.

Slingo JM, Blackburn M, Betts A, Brugge R, Hodges K, Hoskins BJ, Miller M, Steenman-Clark L, Thuburn J. 1994. Mean climate and transience in the Tropics of the UGAMP GCM: Sensitivity to convective parametrization. *Q. J. R. Meteorol. Soc.* **120**: 881–922.

© 2014 The Authors and Crown copyright. *Quarterly Journal of the Royal Meteorological Society* published by John Wiley & Sons Ltd on behalf of the Royal Meteorological Society.

Sperber KR, Palmer TN. 1996. Interannual tropical rainfall variability in general circulation model simulations associated with the atmospheric model intercomparison project. *J. Clim.* **9**: 2727–2750.

Sperber KR, Slingo J, Annamalai H. 2000. Predictability and the relationship between subseasonal and interannual variability. *Q. J. R. Meteorol. Soc.* **126**: 2545–2574.

Sperber KR, Annamalai H, Kang IS, Kitoh A, Moise A, Turner AG, Wang B, Zhou T. 2013. The Asian summer monsoon: An intercomparison of CMIP5 versus CMIP3 simulations of the late 20th century. *Clim. Dyn.* **41**: 2711–2744, doi: 10.1007/s00382-012-1607-6.

Stan C, Khairoutdinov M, Demott CA, Krishnamurthy V, Straus DM, Randall DA, Iii JLK, Shukla J. 2010. An ocean–atmosphere climate simulation with an embedded cloud-resolving model. *Geophys. Res. Lett.* **37**: 1–6, doi: 10.1029/2009GL040822.

Stratton RA, Stirling A, Derbyshire S. 2009. 'Changes and developments to Convective Momentum Transport (CMT) parametrization based on analysis of CRM and SCM'. Technical report 530. Met Office: Exeter, UK.

Terray L. 1998. Sensitivity of climate drift to atmospheric physical parameterizations in a coupled ocean–atmosphere general circulation model. *J. Clim.* **11**: 1633–1658.

Turner AG, Slingo J. 2009. Uncertainties in future projections of extreme precipitation. *Atmos. Sci. Lett.* **10**: 152–158.

Walters DN, Best MJ, Bushell AC, Copsey D, Edwards JM, Falloon PD, Harris CM, Lock AP, Manners JC, Morcrette CJ, Roberts MJ, Stratton RA, Webster S, Wilkinson JM, Willett MR, Boutle IA, Earnshaw PD, Hill PG, MacLachlan C, Martin GM, Palmer MD, Petch JC, Rooney GG, Scaife AA, Williams KD. 2011. The Met Office Unified Model global atmosphere 3.0/3.1 and JULES global land 3.0/3.1 configurations. *Geosci. Model Dev.* **4**: 919–941, doi: 10.5194/gmd-4-919-2011.

World Meteorological Organization (WMO). 1966. *International Civil Aviation Organisation Standard Atmosphere, International Meteorological Tables*. WMO: Geneva, Switzerland.

© 2014 The Authors and Crown copyright. *Quarterly Journal of the Royal Meteorological Society* published by John Wiley & Sons Ltd on behalf of the Royal Meteorological Society.